AFOSR-TR· 9 1 (· 2

②

AD-A238 029

FISSION-FUSION ADAPTIVITY IN FINITE ELEMENTS
FOR NONLINEAR DYNAMICS OF SHELLS

Principal Investigator: Ted Belytschko

Final Report

October 1, 1987 – August 30, 1990

Department of Civil Engineering
Northwestern University
Evanston, Illinois 60208

A-1

The view and conclusions contained in this document are those of the authors and should not be interpreted as necessarily representing the official policies or endorsements, either expressed or implied, of the Air Force Office of Scientific Research or the U.S. Government.

91-04741

REPORT DOCUMENTATION PAGE

1a. REPORT SECURITY CLASSIFICATION UNCLASSIFIED		1b. RESTRICTIVE MARKINGS			
2a. SECURITY CLASSIFICATION AUTHORITY		3. DISTRIBUTION/AVAILABILITY OF REPORT Approved for public release, distribution unlimited			
2b. DECLASSIFICATION/DOWNGRADING SCHEDULE					
4. PERFORMING ORGANIZATION REPORT NUMBER(S)		5. MONITORING ORGANIZATION REPORT NUMBER(S)			
6a. NAME OF PERFORMING ORGANIZATION Northwestern University	6b. OFFICE SYMBOL (If applicable)	7a. NAME OF MONITORING ORGANIZATION USAF, AFSC Air Force Office of Scientific Research			
6c. ADDRESS (City, State and ZIP Code) Department of Civil Engineering The Technological Institute Evanston, IL 60208		7b. ADDRESS (City, State and ZIP Code) Building 410 Bolling AFB, D.C. 20332-6448			
8a. NAME OF FUNDING/SPONSORING ORGANIZATION AFOSR	8b. OFFICE SYMBOL (If applicable) NA	9. PROCUREMENT INSTRUMENT IDENTIFICATION NUMBER F49620-88-C-0011			
8c. ADDRESS (City, State and ZIP Code) AFOSR/NA Bolling AFB DC 20332-6448		10. SOURCE OF FUNDING NOS.			

	PROGRAM ELEMENT NO.	PROJECT NO.	TASK NO.	WORK UNIT NO.
				B1

11. TITLE (Include Security Classification) FISSION-FUSION ADAPTIVITY IN FINITE ELEMENTS FOR NONLINEAR DYNAMICS OF SHELLS			
12. PERSONAL AUTHOR(S) T. Belytschko			
13a. TYPE OF REPORT Final Technical	13b. TIME COVERED FROM 10/01/87 TO 08/30/90	14. DATE OF REPORT (Yr., Mo., Day) 30 November 1988	15. PAGE COUNT 65

16. SUPPLEMENTARY NOTATION

17	COSATI CODES		18. SUBJECT TERMS (Continue on reverse if necessary and identify by block number)
FIELD	GROUP	SUB. GR.	finite elements, adaptive meshes, shells

19. ABSTRACT (Continue on reverse if necessary and identify by block number)

Adaptive methods were studied for localization problems in nonlinear structural dynamics. Localization accompanies failure processes such as hingeline formation in buckling, shearbanding, and fracture. The focus of this study was hingeline formation, but preliminary studies of shearbanding were also made.

From consideration of the advantages and drawbacks of various type of adaptivity, it was determined that an h-method is most suitable for explicit time integration. Refinements accomplished by fission of elements, derefinement by fusion. The error in the flexural energy dissipation was chosen as an error indicator. Results show that the adaptive method is capable of achieving accuracy comparable to that of much finer uniform meshes.

20. DISTRIBUTION/AVAILABILITY OF ABSTRACT UNCLASSIFIED/UNLIMITED ☒ SAME AS RPT. ☒ DTIC USERS ☐	21. ABSTRACT SECURITY CLASSIFICATION UNCLASSIFIED	
22a. NAME OF RESPONSIBLE INDIVIDUAL Professor Ted Belytschko	22b. TELEPHONE NUMBER (Include Area Code) (312) 491-7270	22c. OFFICE SYMBOL NA

DD FORM 1473, 83 APR   EDITION OF 1 JAN 73 IS OBSOLETE.

TABLE OF CONTENTS

PREFACE

This research was conducted under the direction of Professor Ted Belytschko. The following research personnel participated in the research program: Dr. Bak Leong Wong, Mr. Lee Bindeman and Mr. Edward J. Plaskacz.

T. Belytschko, B.K. Wong, and H. Stolarski, "Assumed Strain Stabilization Procedure for the 9-Node Lagrange Shell Element," International Journal for Numerical Methods in Engineering, 28, 385-414, 1989.

Y.J. Wang and T. Belytschko, "A Study of Stabilization and Projection in the 4-Node Mindlin Plate Element," International Journal for Numerical Methods in Engineering, 28, 2223-2238, 1989.

T. Belytschko and D. Lasry, "A Study of Localization Limiters for Strain-Softening in Statics and Dynamics," Computers and Structures, 33(3), 707-715, 1989.

M. R. Ramirez and T. Belytschko, "An Expert System for Setting Time Steps in Dynamic Finite Element Programs," Engineering with Computers, 5, 205-219, 1989.

T. Belytschko, B.L. Wong, and E.J. Plaskacz, "Fission-Fusion Adaptivity in Finite Elements for Nonlinear Dynamics of Shells," Computers and Structures, 33(5), 1307-1323, 1989.

T. Belytschko, B.L. Wong, and H.Y. Chiang, "Improvements in Low-Order Shell Elements for Explicit Transient Analysis," to appear Computer Methods in Applied Mechanics and Engineering.

J. Donea and T. Belytschko, "Advances in Computational Mechanics," to appear Nuclear Engineering and Design.

T. Belytschko and J.-S. Yeh, "H-Adaptive Methods with Contact-Impact," in preparation.

The following doctorates were supported by this research:

Bak Leong Wong, "Shell Finite Elements: A New Resultant Stress Formulation and Stabilization, " December 1987.

Edward J. Plaskacz, "Fission-Fusion Adaptivity in Finite Elements for Nonlinear Dynamics of Shells," June 1990.

1. INTRODUCTION

The objective of this work was to develop adaptive finite element methods for nonlinear structural dynamics. Adaptive methods are particularly promising for nonlinear problems involving failure, because in failure and near-failure states of structures, three phenomena are predominant;

    1. buckling

    2. shear banding

    3. fracture.

All of the above phenomena are associated with localization of the deformation, by which is meant the development of large strains in small regions of the structure, which is accompanied by large gradients in the strain. For example, while strains are rather distributed in elastic buckling, once plasticity develops a large part of the deformation of a beam or shell usually occurs over narrow zone called a hingeline. Shear banding is a result of strain softening material behavior and is also associated with very narrow ʼ ands of highly strained material. In specimens ranging in size from 0.11 to 1.0 meter, shear band widths are of the order of 10 to 100 microns. In fracture, high strain gradients occur at the crack tip, and in addition the displacement field is discontinuous behind the crack tip.

Because of the localization of deformation in these problems, it is clear that uniform meshes will be quite ineffective. Although some analysts have sufficient intuition to guess where the localization will occur, generally it cannot be known a priori.

For these reasons, it seems that adaptive methods are essential in the solution of nonlinear problems. However, perusal of the reviews of the field of adaptive finite elements by Noor and Babuska (Ref. 1) and Oden and Demkowicz(Ref. 2) shows that the majority of the work has been devoted to linear problems.

In this work, adaptive methods are developed for the nonlinear dynamics of shells with both geometric and material nonlinearities. The localization phenomenon which is of

primary interest in this class of problems is hingeline formation, but aspects of this work should be applicable to other localization phenomena in structural dynamics. In order to simplify data management, an explicit time integration algorithm was chosen. By focusing the research on explicit time integration, the research should be relevant to a large class of widely used programs such as DYNA3D.

There are three types of mesh adaptivity:

1. r-adaptive;

2. h-adaptive;

3. p-adaptive.

In the r-method, nodes are relocated in order to place most of the resolution in the areas where they are needed. This corresponds in fact to Arbitrary Lagrangian-Eulerian methods; these were studied in this research and reported in Ref. 3. However, r-methods were found to be unsatisfactory for treating localization phenomena for 3 reasons:

1. in moving the nodes to areas of high strain gradients, the elements become severely distorted, which compromises their effectiveness;

2. it is difficult to obtain sufficient resolution by simply moving nodes;

3. in shell problems, it is difficult to maintain fidelity in the modeling of the shape of the shell as the nodes move.

In p-methods, resolution is increased where it is needed by increasing the order (or power) of the interpolants. This method was deemed inappropriate for explicit dynamics methods for two reasons:

1. it is difficult to construct an accurate diagonal mass for higher order elements and explicit methods rely for their efficiency on the avoidance of triangulating a nondiagonal mass matrix;

2. higher order elements results in very small critical time steps and rather noisy solutions result when used with explicit integration.

In an h-method, elements are subdivided where greater resolution is needed. We will call this process fission. In addition, in dynamic problems it is possible to conserve resources by fusing those elements which are no longer actively deforming. An advantage of the method is that it is possible to allocate a large number of unknowns in a small subdomain without mesh distortion or introducing higher order elements. The h-method has the disadvantage that the critical time step of the mesh decreases dramatically after several levels of fission, but this can be overcome by using different time steps in different parts of mesh.

Based on these factors, we concentrated on the h-method. This method briefly summarized in Section 2. Section 3 gives some examples obtained by these methods and Section 4 summarizes the research and discusses future directions.

2. SUMMARY OF METHODOLOGY

The methodology is described in Refs. 3 and 4. In this Section, some of the issues are briefly reviewed. An explicit finite element program for the nonlinear transient analysis of shells was used as the framework for the research. A one-point quadrature shell element which Hallquist in DYNA3D manuals calls the Belytschko-Tsay element(Ref. 5) was used. We encountered some difficulties with this element so they were rectified as described in Appendix A. As indicated in Fig. 1, the h-method consists of two processes:

1. fission of a quadrilateral element into 4 elements when more refinement is needed;

2. fusion of four quadrilaterals into a single quadrilateral when activity has ceased in a subdomain.

The fission-fusion processes are triggered by error criteria. In this work we have studied two error criteria:

1. the error in the flexural dissipation rate due to errors in the approximation of the transverse displacement;
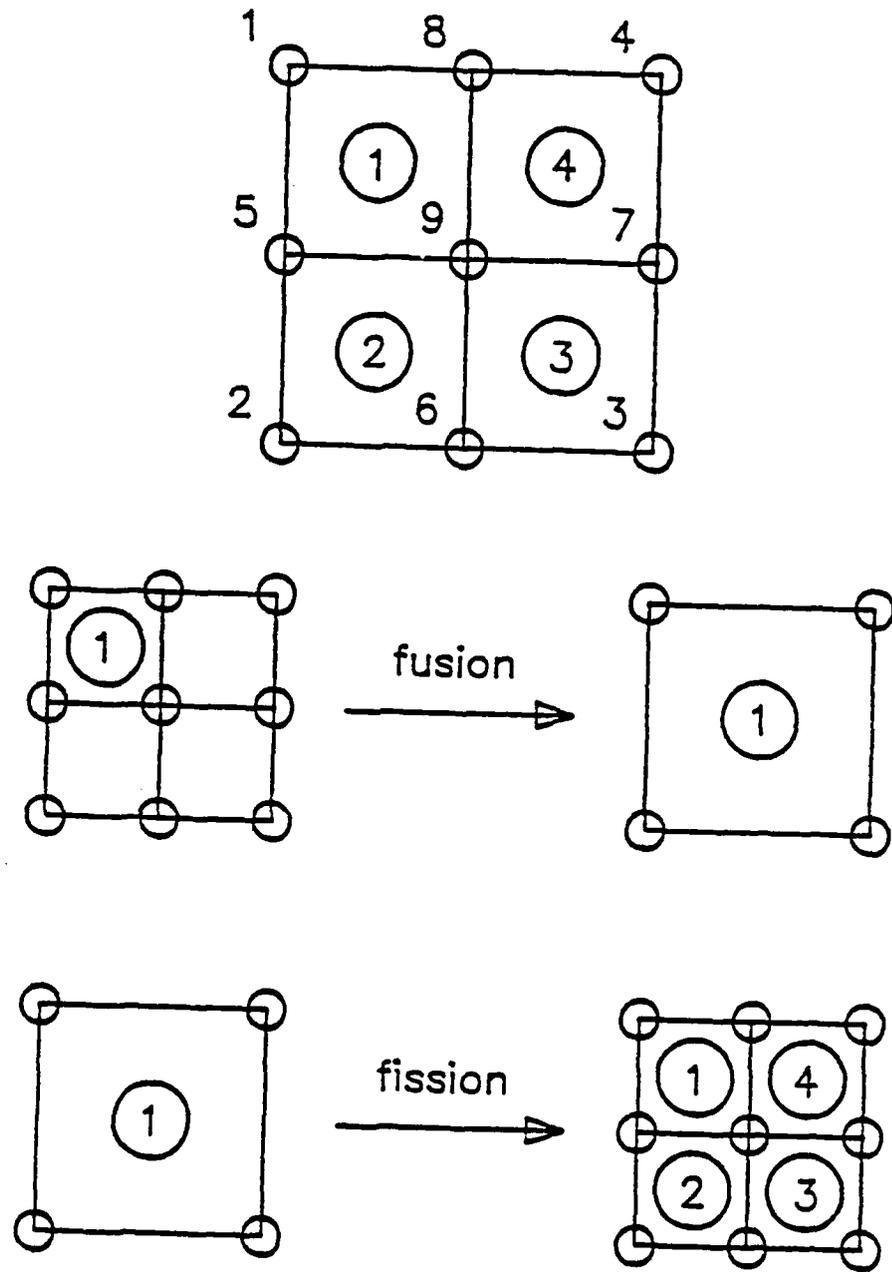
-3

Figure   1.   Depiction of fusion and fission processes in h-adaptivity.

2. the error in energy due to one-point quadrature.

It has also been attempted to combine the two methods by using the rates of dissipation associated with the two types of errors.

The studies have shown that the first error criterion, error in flexural energy dissipation, as measured by the energy dissipated by the discontinuity in slope between two elements, is the more effective. Furthermore, it has been difficult to derive error criteria which are effective for the combined energies.

Another aspect of adaptive methods in transient analysis is that error criteria should only be applied at selected intervals of the time integration process. If the error criteria and adaptation is attempted every time step, then the fission-fusion process becomes oscillatory, i.e. fission in an element or group of elements is rapidly followed by fusion. This occurs because the fission process reduces the error in a group of elements dramatically, and if the errors in these elements are now compared to the remainder of elements, the error tends to fall near the bottom.

One technique which has been successful in eliminating this churning is to consider the error criteria over groups of elements. In other words, instead of using an error indicator that pertains to a single element, the error is evaluated over a group of elements and then normalized by the volume of elements.

A second technique we have found very useful is to limit the adaptation process to selected time steps. For example, in the problems that have been studied here, limiting the adaptation process to every 50 time steps increases the efficiency and improves the conditioning of the solution. The latter occurs because adaptation tends to introduce noise in the numerical solution. However, when the number of time steps between adaptation is moderately large, backtracking, where the integration from the previous adaptation is repeated with the new mesh, is useful.

One aspect of an h-adaptive method that requires considerable work is the data structure. It is necessary to keep track of the elements from which an element originated,

and the siblings(elements formed by the same fission). In multilevel adaptivity, this information must be available for several generations. To accomplish this task, a data structure similar to that of Devloo, et al.(Ref. 6) was used. However, it was modified so that it is more easily vectorizable.

It is not clear whether h-adaptive methods will be successful in resolving shear bands in metallic structures. Shear bands in a specimen of size 10^{-1} m are often of the order of 10 microns(10^{-5} m). If it is desired to capture any of the structure of the shear band, then meshes with at least 5 to 10 elements across the band will be needed. This entails elements with h = 10^{-6}. Even if elements of this size are used only on the band itself, more than 10^6 elements would be needed(10 element across the band by 10^5 elements along the band plus elements for the rest of the mesh). Therefore, some type of directional p-refinement or methods such as the spectral overlay may be more suitable.

3. NUMERICAL EXAMPLES

In this section, some of the numerical results obtained by the adaptive methods will be described. Since closed-form solutions are not available for nonlinear transient problems, two types of comparisons are used for the adaptive solutions:

1. numerical results obtained by finer meshes;

2. experimental results.

The first example is a cylindrical panel which is impulsively loaded over the top by an explosive sheet in the area indicated in Fig. 2. Deformed mesh plots for the finer adaptive mesh are shown at various times in Figs 3 and 4. Here the incremental transverse bending energy is used for the fission-fusion criterion. It can be seen that after 0.0125 msec, the crown settles downward like a plateau and the fissioning process migrates laterally towards the line where the curvature is maximum. During this time, the crown moves down in a frozen plateau-like state. After that, the crown develops a convex curvature when viewed from above, and the elements in the crown are again fission-fusion,
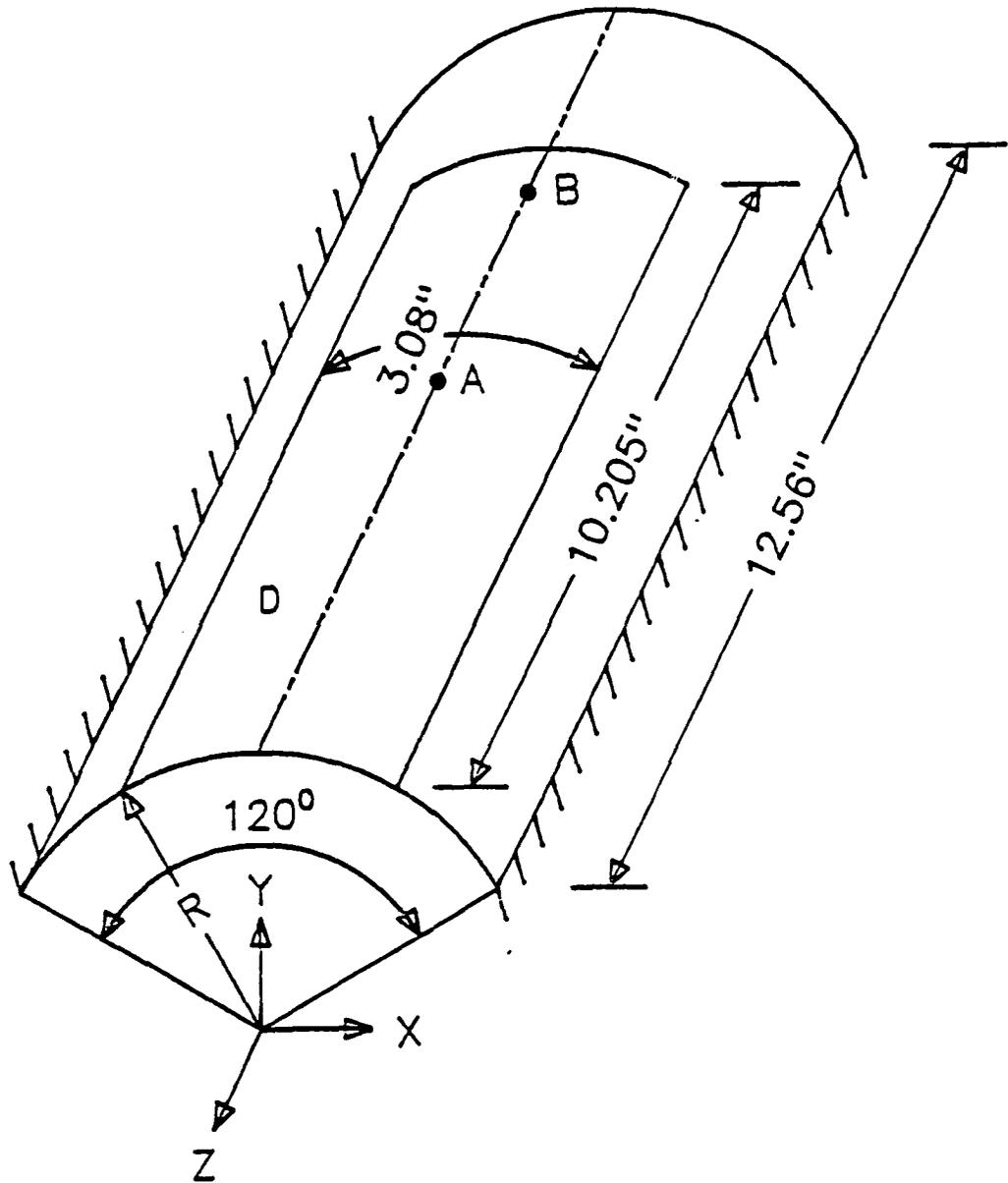
Figure   2.   Impulsively loaded cylindrical panel; initial velocity is applied
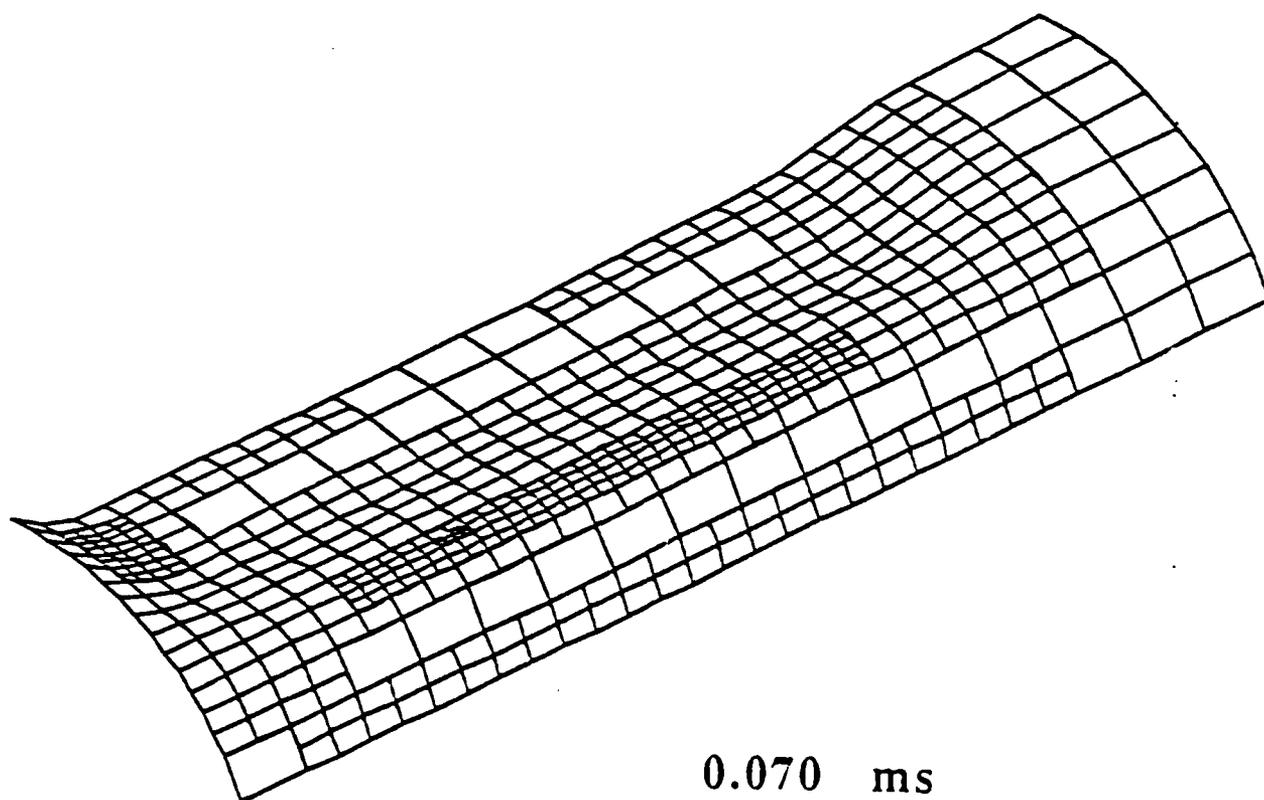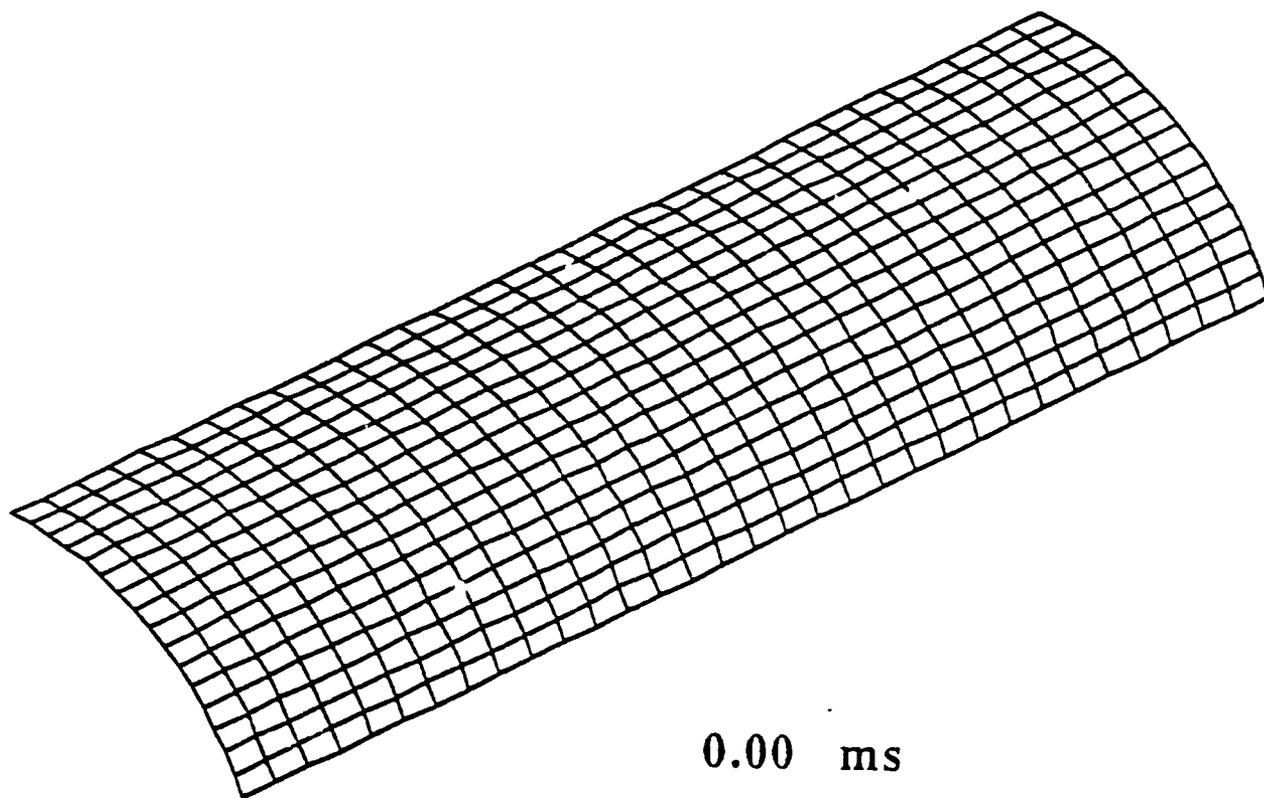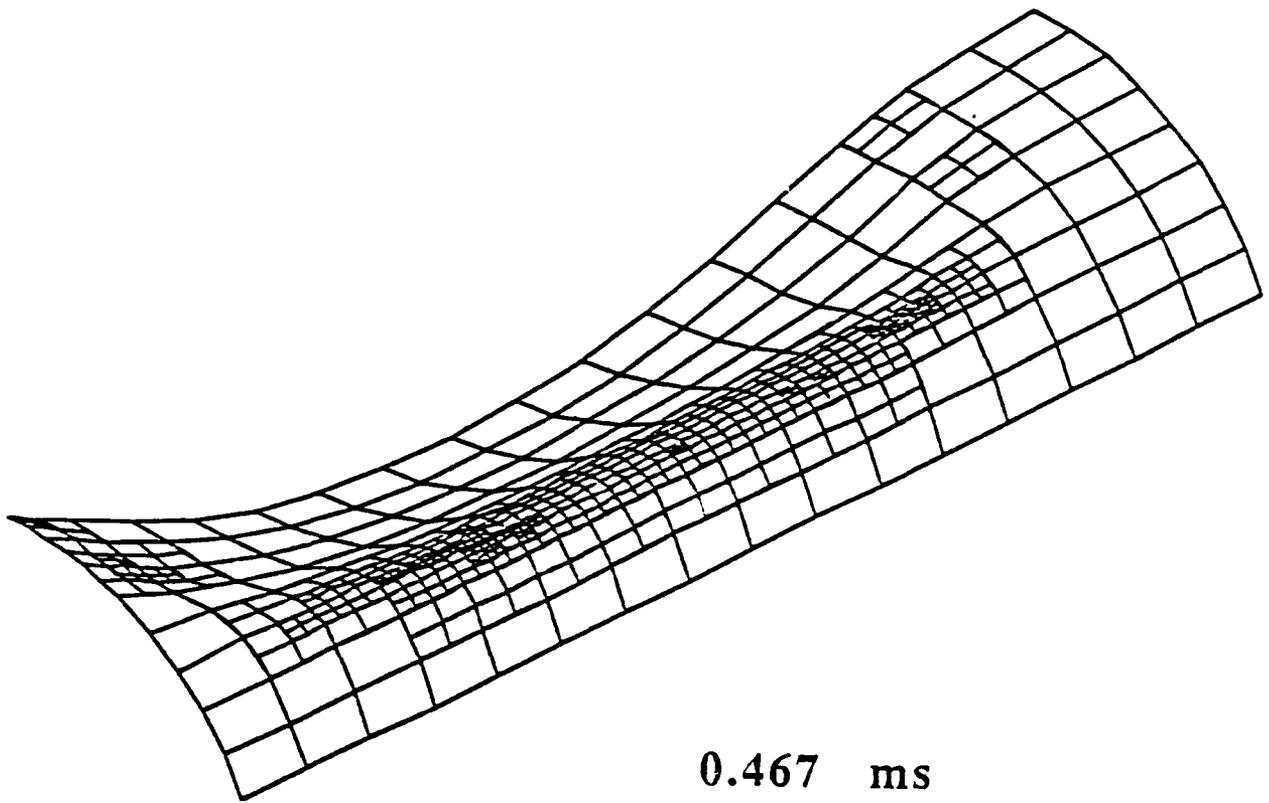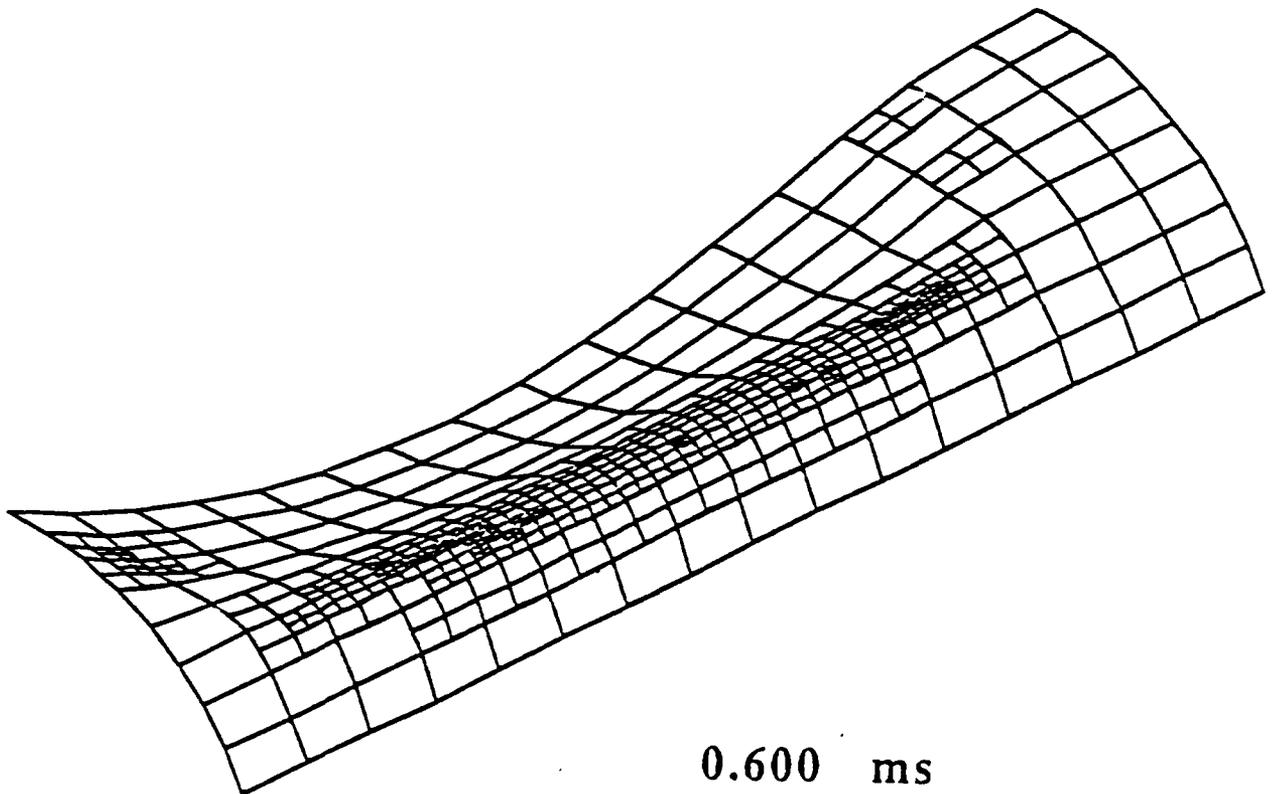over domain D.

0.00 ms

0.070 ms

Figure 3. Initial and deformed mesh for the cylindrical panel with multi-level adaptivity.

0.467 ms

0.600 ms

Figure 4.   Deformed meshed for the cylindrical panel.

which is a tendency that needs to be fixed: it is probably due to the fact that the incremental work is quite small in the later stages because most of the deformation has taken place, so the incremental work is quite uniformly distributed, allowing the fission-fusion process to be triggered by small oscillations in the solution.

The time histories of the displacement at two points obtained by the h-adaptive method are compared to the experimental results in Fig. 5 and 6. Experimental results have been obtained for this shell by Morino, Leech, and Witmer(Ref. 7), who report a maximum deflection of 1.27 in. at point A. The first fixed and adaptive meshes yield maximum deflections of 1.17 and 1.24 in., respectively. These results show that even two-level adaptivity is quite successful.

To illustrate the effectiveness of the adaptive method more clearly, Table 1 gives the results for the maximum displacements at points A and B for various uniform meshes and the adaptive meshes. The finest meshes were run on a Connection Machine(CM) implementation of the program and would not be feasible on a CRAY. It is apparent with

| Mesh for half-panel	Description	Maximum Displacement (inch) at	
		n = -6.2	n = -9.42
6x16	uniform	1.001	0.494
8x16	uniform	1.106	0.526
10x20	uniform	1.126	0.527
12x24	uniform	1.146	0.531
16x23	uniform	1.194	0.585
512	3 level adaptive	1.234	0.606
64x128	uniform CM	1.264	0.636
64x256	uniform CM	1.261	0.631
128x256	uniform CM	1.264	0.636
Experimental	Balmer and Witmer (1964)	1.28	0.68

Table 1. Cylindrical Panel Results
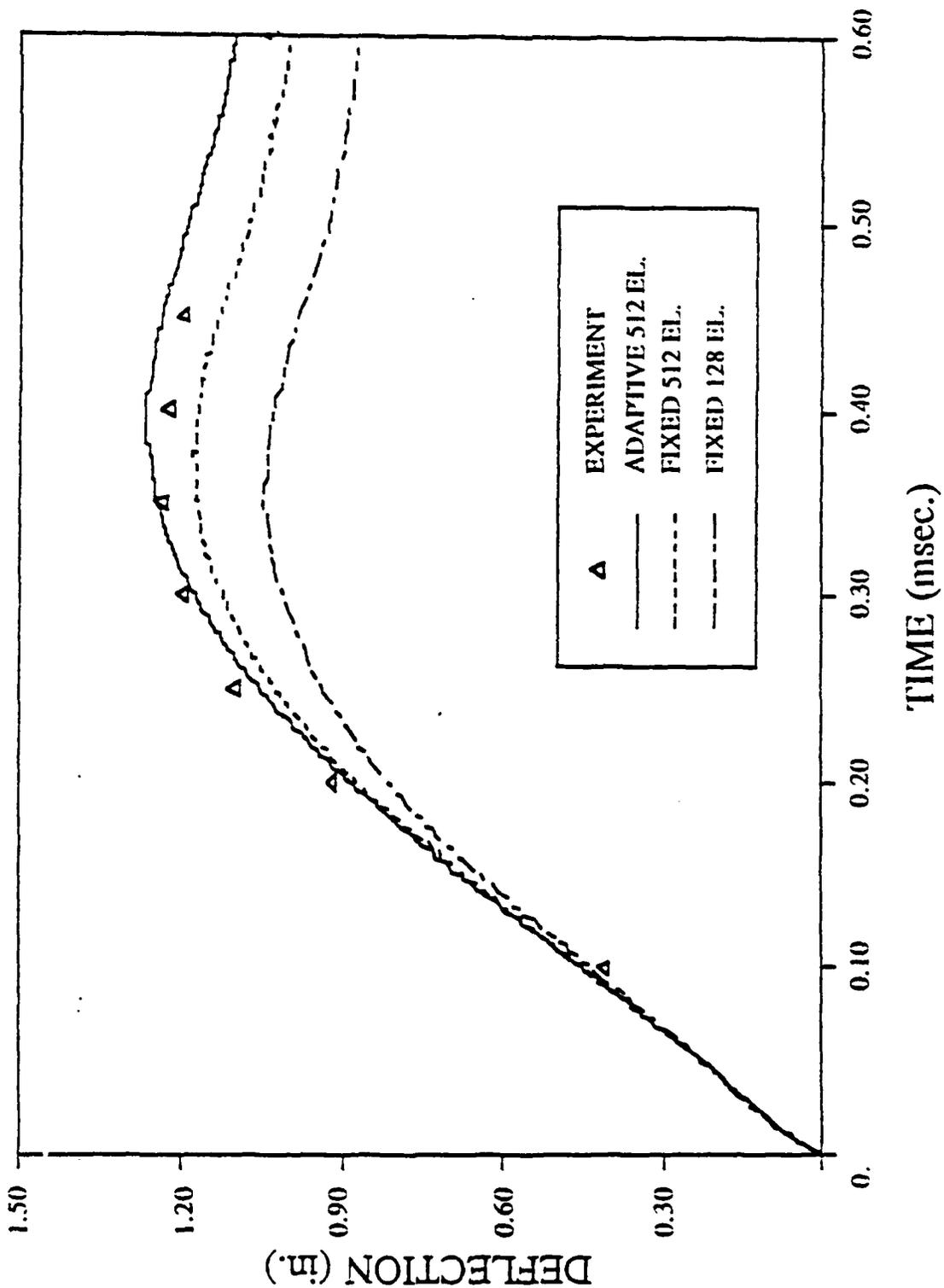
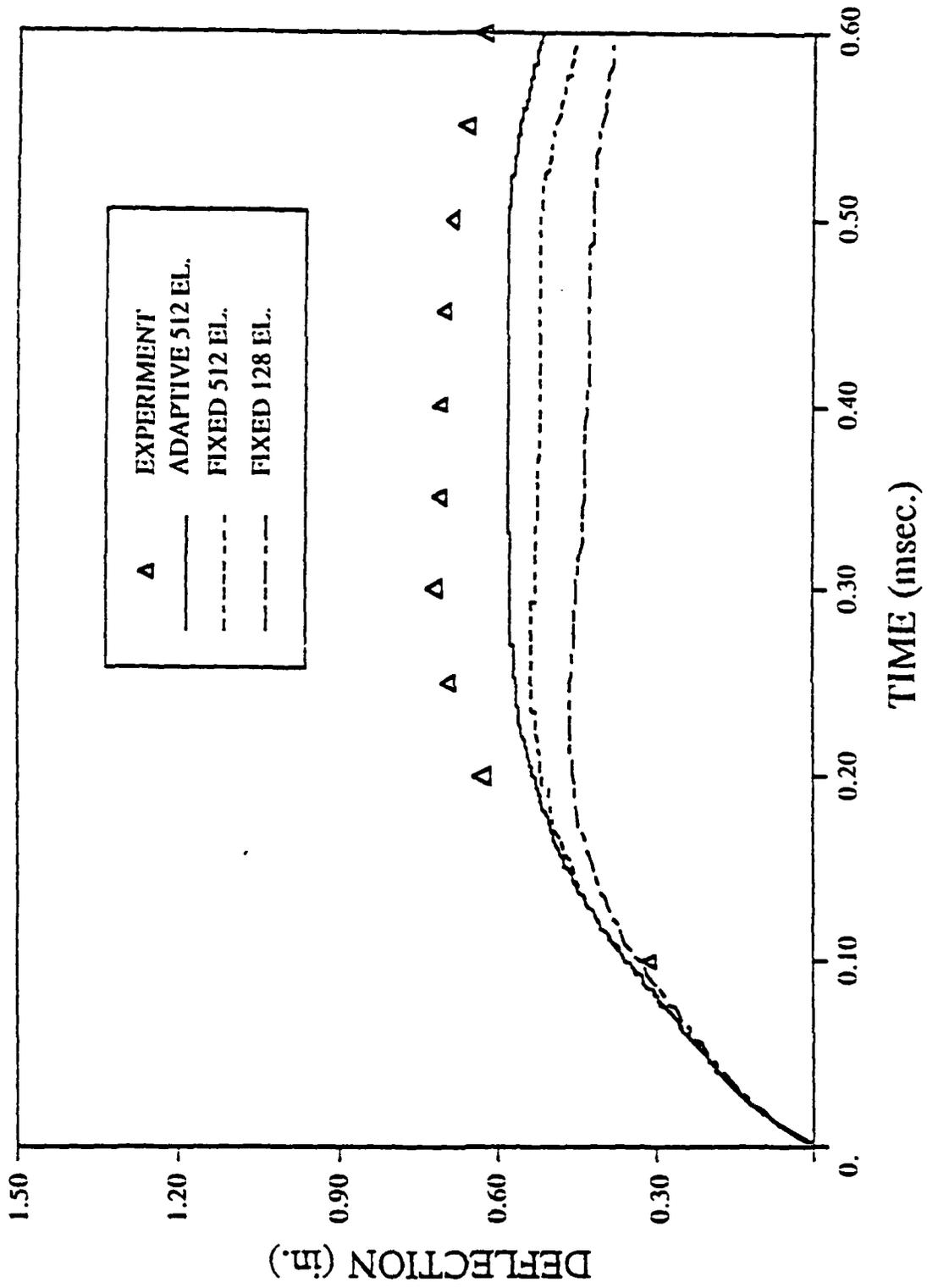Figure 5. Displacement time history of node A of the cylindrical panel with multi-level adaptivity.

Figure 6. Displacement time history of node-B of the cylindrical panel with multi-level adaptivity.

these extremely fine meshes, a converged solution has been obtained. The converge solution does not agree exactly with the experimental solution, and while the ultimate test of a computation is agreement with experimental results, in nonlinear problems it is difficult to distinguish errors arising from deficiencies in the constitutive models, boundary modeling and loading from errors due to insufficient mesh resolution. In the CM runs, resolution is apparently no longer an issue, so these results can be considered a benchmark for this problem. It is interesting to observe how slowly uniform meshes converge to this benchmark. Even a 12×24 mesh(for half of the panel) is more than 10% in error; many results reported in the structure involve even coarser meshes. On the other hand an adaptive mesh with the same member of elements is only 4% in error.

The second example is a hollow, cylindrical column which is subjected to a compressive axial load. This problem is of interest because it exhibits both global and local buckling, the latter resulting in buckling of the cross section. Numerical results and experimental results are reported for this problem by Kennedy, Belytschko, and Liu(Ref. 8).

The cylinder is loaded by prescribing an upward velocity of 500 in/sec to the bottom nodes of the model, with the top fixed. To trigger the lateral buckling mode, an imperfection given by

$$\Delta x = 0.01 \sin \frac{2\pi z}{\ell}$$

where ℓ is the length of the column and z is the coordinate along the axis of the column, is added to the x-coordinate of all nodes.

The problem is solved with multi-level adaptivity and the transverse energy criterion. The pattern of adaptivity is shown in Fig. 7. Initially, the fission process is only one level and occurs at the eventual extreme of the buckling wave. The important point to note is that the fission process then focuses at the points of local buckling.
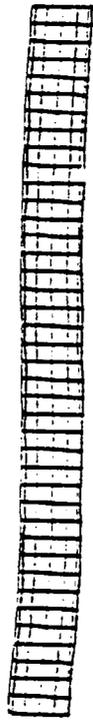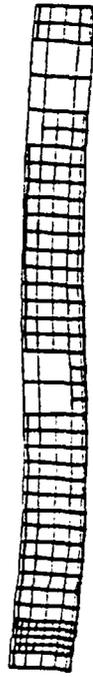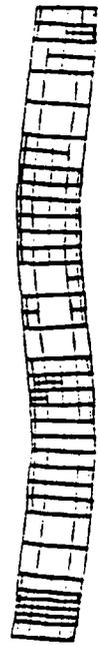
0.0 msec   0.17 msec   0.30 msec
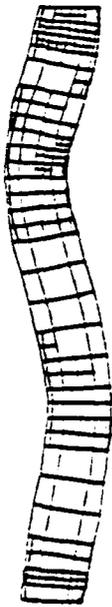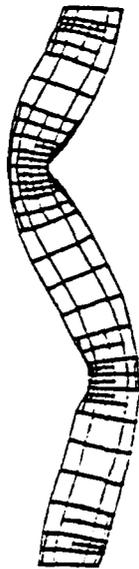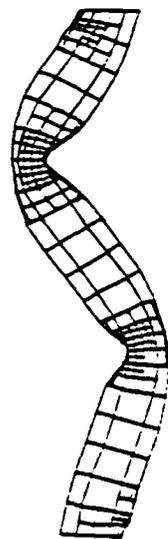
0.47 msec   0.64 msec   0.80 msec

Figure   7.   Deformed adaptive meshes for the cylindrical column with multi-
level adaptivity.

-14-

Another class of example we have studied is shear banding. H-adaptivity was not successful here so we developed a new method which is in a sense p-adaptive. In this method, the resolution is increased by overlaying the finite element mesh with a spectral interpolant in a zone that coincides with the shear band. The results for a tensile specimen, shown in Fig. 8, are given in Figs 9 to 11. The noteworthy results are the complex structure of the shear band. The sequential times A, B and C are indicated in these figures. Most of the evolution of the shear band takes place between B and C. Note that the shear band has considerable structure, and as can be seen from Fig. 11, its width is of the order of several hundred microns. This is larger than observed physically but much smaller than the element size. We have since learned that the width is determined by the scale of imperfections.

4. SUMMARY AND DISCUSSION

The results have shown that an adaptive mesh can dramatically improve accuracy for a transient, nonlinear finite element solution. Comparison of results for the cylindrical panel with a converged solution obtained on a massively parallel computer on a very large mesh of 16K elements show that the h-adaptive method can obtain similar accuracy with 528 elements, whereas a uniform mesh of this size is in error in the maximum displacement by almost 10%.

A key finding of this work is that the error criteria generally used in linear analysis are not well suited for problem of localization in nonlinear mechanics. The difficulty arises because linear error criteria, such as that of Zienkiewicz and Zhu consider the difference between a C^0 least-square fit to the stresses and the C^{-1} stress field obtained by the finite element scheme; the error criteria of Babuska relate the error to the jumps in the stress fields at element interfaces, but give similar results. In localization, such as buckling and shear banding, the stress field is very homogeneous, so the difference between the C^0 and C^{-1} fields(and the jumps in the stresses at element interfaces) are small. Thus these error
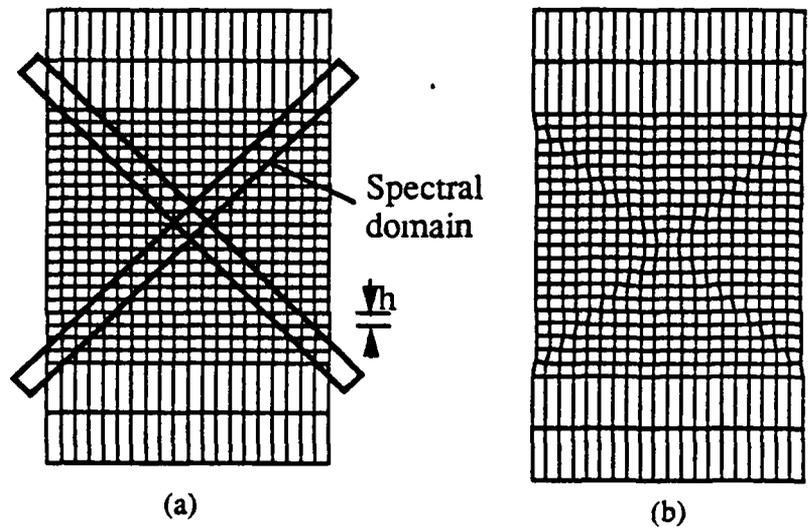
Figure   8.   Undeformed mesh for the rectangular tensile specimen with spectral patch superimposed and deformed mesh.
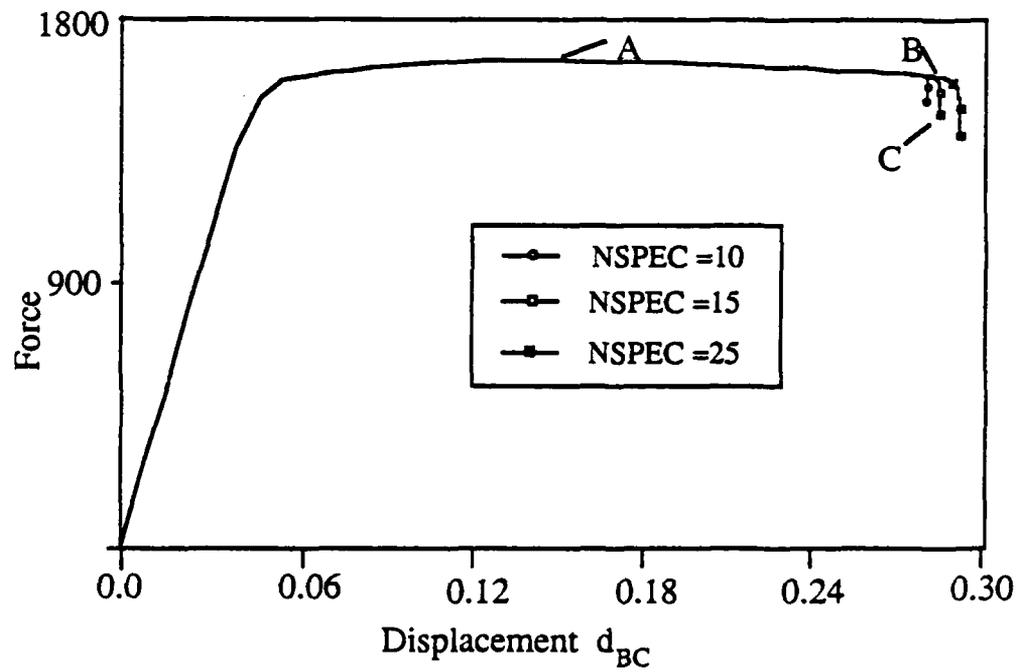
Figure   9.   Force-displacement curves for rectangular tensile specimen with various degrees of resolution in the spectral overlay.
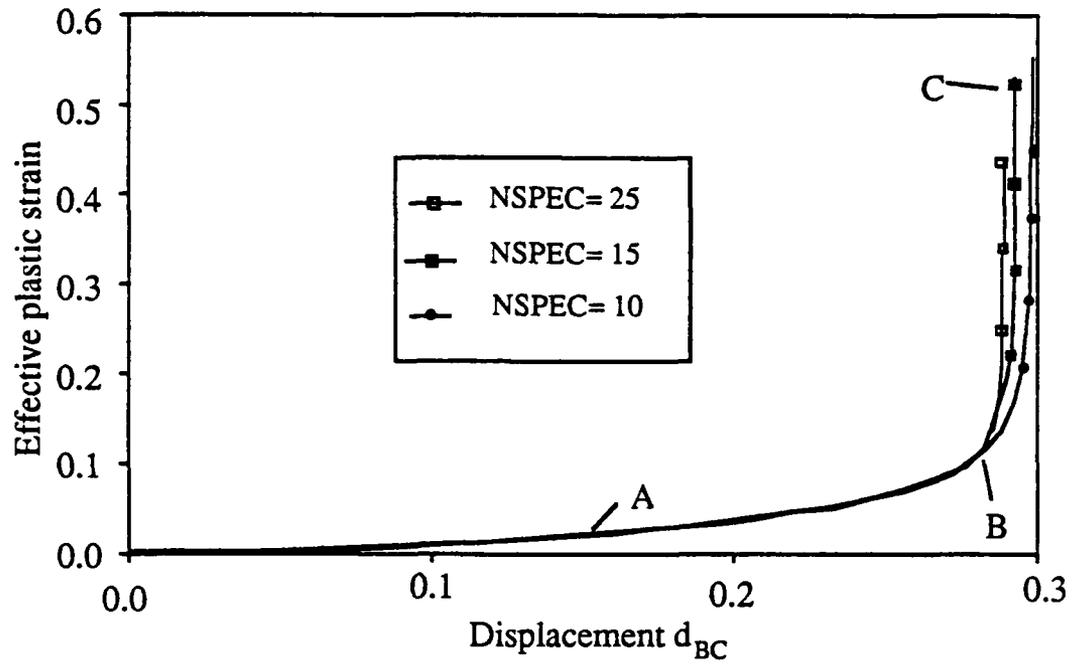
Figure 10.   The **maximum** effective plastic strain in the shear band as a function of the displacement of the ends of the specimen.
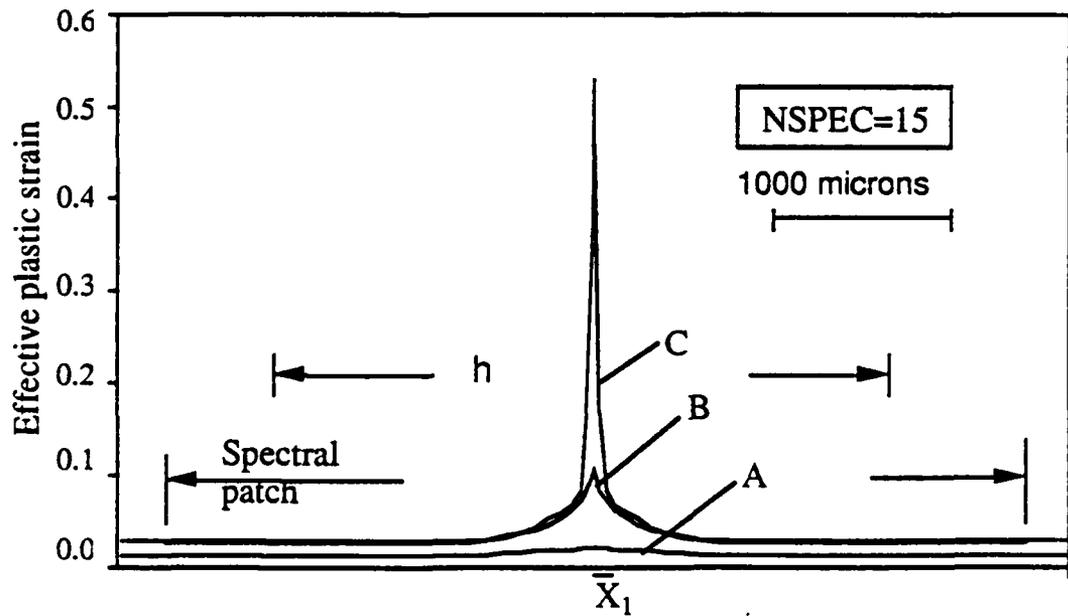
Figure 11.   Effective plastic strain in a cross-section across the shear band.

criteria will not be successful in determining where to refine the mesh. It appears the development of refinement criteria for such problems may be accomplished most effectively if the physics of the phenomena which are expected are used as guideline. Thus in this study, where hingeline formation was of interest, we used the flexural energy as an error indicator. Although such approaches would not be suitable for completely automatic adaptive computation of nonlinear problems, it has appeal for skilled analysts.

In this study, the localization phenomena considered was the formation of elastic-plastic hingelines associated with buckling. The application of these techniques to other localization phenomena requires further work. In particular, error criteria appropriate for other types of localization need to be devised. The error criteria developed here are not universally applicable to nonlinear problems. Considerable additional work is needed on error criteria if adaptive methods are to be usefully applied to nonlinear structural problems with localization. Since accurate resolution of localization is the major reason for applying adaptive methods to nonlinear structural problems, unless error criteria are developed, adaptivity will not be successful.

To avoid excessive churning of the fission-fusion process, time delays had to be incorporated in the judgment process. Thus, fission and fusion are executed only when indicated by two or more consecutive judgment. Nevertheless, churning becomes a problem with the incremental dissipation criterion in the later stages of impulsively loaded problems when the work on the system decreases; rational methods of controlling it need to be developed.

The h-adaptive procedure is limited in its ability to resolve the subdomains of maximum deformation by the fact that the parent element configuration is fixed. Therefore, hinge lines which occur at angles relative procedure to the mesh lines may not be captured effectively. However the h-method appears to be the best compromise between simplicity and effectiveness in the solution of nonlinear structures by explicit methods. The results we have obtained show that these adaptive schemes are capable of achieving substantial

improvements in accuracy for a given computational effort. Generally, an adaptive mesh is capable of achieving the same accuracy with less than half of the computational resources. The fission process tends to take place in the subdomains where the maximum deformation occurs.

In this study, an h-method was selected because of its advantages in an explicit integration algorithm. However, further study on quadratic element technology has indicated that effective 9 node elements can be developed with 4 quadrature points. It has also been found that by iterating on the off-diagonal terms of the mass matrix only once or twice, it is possible to obtain good solutions to transient problems with these higher order elements without triangulating the complete consistent mass. Therefore p-method deserves further consideration in these problems.

REFERENCES

1. J. T. Oden and L. Demkowicz (1988). "Advances in Adaptive Improvements: A Survey of Adaptive Finite Elements in Computational Mechanics", in State of the Art Surveys in Computational Mechanics, ed. A. K. Noor et el, ASME, New York, in press.

2. A. K. Noor and I. Babuska (1987). "Quality Assessment and Control of Finite Element Solutions", Finite Elements in Analysis and Design, 3(1), 1-26.

3. W. K. Liu, H. Chang, J. S. Chen, and T. Belytschko (1988). "Arbitrary Lagrangian-Eulerlian Petrov-Galerkin Finite Elements for Nonlinear Continua", Computer Methods in Applied Mechanics and Engineering, 68(3), 259-310.

4. T. Belytschko, B. L. Wong, and H. Y. Plaskacz (1989). "Fission-Fusion Adaptivity in Finite Elements for Nonlinear Dynamics of Shells", Computers and Structures, 33(5), 1307-1323.

5. T. Belytschko, J. I. Lin, and C. -S. Tsay (1984). "Explicit Algorithms for the nonlinear Dynamics of Shells", Computer Methods in Applied Mechanics and Engineering, 42, 225-251.

6. P. Devloo, J. T. Oden, and T. Stroubelis (1987). "Implementation of an Adaptive

Refinement Technique for the SUPG Algorithm", Computational Methods in Applied Mechanics and Engineering, 61, 339-358.

7. L. Morino, J. W. Leech, and E. A. Witmer (1971). "An Improved Numerical Calculation Technique for Large Elastic-Plastic Transient Deformations of thin Shells: Part 2 - Evaluation and Applications", Journal of Applied Mechanics, 38(2), 429-436.

8. J. M. Kennedy, T. Belytschko, and J. I. Lin (1986). "Recent Developments in Explicit Finite Element Techniques and Their Application to Reactor Structures", Nuclear Engineering and Design, 97(1), 1-24.

APPENDIX A

1. INTRODUCTION

Four-node quadrilateral shell elements with one quadrature point in the mid-surface have become widely used in programs with explicit time integration. The first of these elements was described by Belytschko and Tsay (Ref. 3); also see Belytschko, Lin and Tsay (Ref. 4). This element is used in DYNA3D, PAMCRASH and other programs developed for crashworthiness studies. Hallquist (Ref. 7) also adapted the Hughes and Liu (Refs. 8 and 9) shell element to these programs by adding an hourglass control similar to that in Ref. 4.

The major objective in the development of the Belytschko-Tsay element was to attain a convergent, stable element with the minimum number of computations. For this reason, the element uses bilinear isoparametrics with one quadrature point in the mid-plane when the material is elastic. If the material is nonlinear, several quadrature points are used through the thickness at a single mid-plane point. Because this element with one-point quadrature would be rank deficient, i.e., it would possess so-called "hourglass modes" or "spurious singular modes", an hourglass control is added. This hourglass control is orthogonal to all linear fields (see Belytschko and Tsay (Ref. 3) and Belytschko, Lin and Tsay (Ref. 4)), so the consistency for linear fields is not impaired.

Because of the emphasis on speed, several shortcuts were made in formulating the element equations. On the whole, the element has performed quite well, but it has two shortcomings:

1. It performs poorly when warped, and in particular, it does not correctly solve the twisted beam problem.

2. It does not pass the quadratic Kirchhoff-type patch test in the thin plate limit.

The latter shortcoming is shared by the Hughes-Liu element, and its importance was not realized until recently.

In this paper, modifications to the Belytschko-Tsay element which overcome these drawbacks are described. The first shortcoming is eliminated by adding terms into the strain-displacement equations which couple the curvatures to the translations: these terms are shown to be essential to obtaining the correct response when the shell is twisted and the mid-plane shape depends strongly on the bilinear term.

The second shortcoming is eliminated by adding a nodal projection to the shear calculation. The concept of a projection operator to improve element performance was originated by Belytschko, Stolarski and Carpenter (Ref. 5) and studied in a quadrilateral by Stolarski, Carpenter and Belytschko (Ref. 15). The particular projection used here is similar to that developed independently by Hughes and Tezduyar (Ref. 10) and MacNeal (Ref. 12).

In addition, we describe an implementation of the patch test for explicit dynamic programs. The patch test is usually defined in terms of a static analysis, which is not possible with a program that includes only explicit time integration. The patch test described here can be used directly in explicit programs without any modification, so it should prove useful.

This element formulation is based on the "resultant stress theory" (Liu, et al. (Ref. 11) and Stanley (Ref. 14)). The starting point is the degenerated continuum (DC) approach to shells which describes the shape and kinematics (Ref. 8). The strains are then expressed in terms of membrane strains and curvatures. The advantage of resultant stress theories over DC shell

elements is that the number of computations is substantially smaller, which provides significant speed advantages in explicit computer programs.

The paper is organized as follows: In Section 2, the starting point, the DC shell geometry and interpolation are reviewed along with the corotational coordinate system used in this element. Section 3 describes the new kinematic relations; two methods are presented, one requires a knowledge of the pseudonormal vectors, the second does not. Section 4 describes the shear projection. Section 5 describes the implementation of the element, giving the rate-of-deformation-velocity equation. Section 6 gives some numerical results which contrast the performance of this element with the earlier element; a recipe for performing the patch test in explicit programs is also given.

2. GEOMETRY AND INTERPOLATION

In DC shell theories, the coordinates of the shell are given by:

$$x = \frac{1}{2} \sum_{I=1}^{m_e} \left[x_I^{top}(1+\zeta) + x_I^{bot}(1-\zeta) \right] N_I(\xi,\eta) \tag{1a}$$

$$= \sum_{I=1}^{m_e} N_I(\xi,\eta) \left[\frac{1}{2} \left(x_I^{top} + x_I^{bot} \right) + \frac{\zeta}{2} \left(x_I^{top} - x_I^{bot} \right) \right] \tag{1b}$$

$$x_I^T = (x_I, y_I, z_I) \tag{1c}$$

Thus, if we define the pseudonormal at each node I by:

$$p = \left(x_I^{top} - x_I^{bot} \right)_{,I} h_I \tag{2}$$

where h_I is the distance between the two nodes (or a pseudo-thickness at node I), and define the nodes on the mid-surface by:

$$x_I = \frac{1}{2} \left(x_I^{top} + x_I^{bot} \right) \tag{3}$$

then:

$$x = \sum_{I=1}^{m_e} x^m + \bar{\zeta} p \tag{4a}$$

$$= \sum_{I=1}^{m_e} (x_I + \bar{\zeta} p_I) N_I(\xi,\eta) \tag{4b}$$

where:

$$\bar{\zeta} = \frac{\zeta h}{2} \tag{5}$$

and

$$x^m = \sum_{I=1}^{m_e} x_I N_I(\xi, \eta) \qquad (6)$$

In the above, m_e is the number of element nodes, N_I are the shape functions, and h is the pseudo-thickness. Uppercase indices refer to nodal numbers. The superscripts "top" and "bot" refer to the top and bottom nodes which describe the actual continuum, whereas the superscript "m" refers to the mid-surface; nodal coordinates without superscripts pertain to the midsurface. The geometry is shown in Fig. 1.

The element corotational system $(\hat{x}, \hat{y}, \hat{z})$ is constructed as shown in Fig. 2. The mid-points of the sides are connected by lines, r_{ac} and r_{bd}, as shown. The direction of the $\hat{z}$ coordinate, which corresponds to the unit vector $\hat{e}_3$, is then obtained by:

$$\hat{e}_3 = \frac{r_{ac} \times r_{bd}}{\| r_{ac} \times r_{bd} \|} \qquad (7)$$

The precise orientation of the two other unit vectors is usually not important; we choose:

$$\hat{e}_1 = r_{ac} / \| r_{ac} \| \qquad (8)$$

$$\hat{e}_2 = \hat{e}_3 \times \hat{e}_1 \qquad (9)$$

The choice of the unit normal $\hat{e}_3$ is also not critical, but this particular choice has an interesting consequence. Because the two lines r_{ac} and r_{bd} lie in the surface of the isoparametric element, the vector e_3 is exactly normal to the mid-surface at the origin of the reference plane. By contrast, when $\hat{e}_3$ is the cross-product of the diagonals of the element as in Belytschko, Lin and Tsay (Ref. 4), then $\hat{e}_3$ is not exactly normal to the element surface, which complicates some of the subsequent developments. The practical effects are probably not important.

The mid-surface of the shell is given by:

$$\hat{z} = \sum_{I=1}^{4} N_I(\xi, \eta) z_I \qquad (10)$$

where $N_I(x, h)$ are the usual bilinear isoparametric shape functions, which are given by:

$$N_I = \frac{1}{4}(1 + \xi_I \xi)(1 + \eta_I \eta) \qquad (11)$$

The velocity of the shell is obtained from Eq. 4:

$$v \equiv \dot{x} = v^m + \bar{\zeta}\dot{p} \qquad (12a)$$

$$v^m \equiv \dot{x} \qquad (12b)$$

Superposed dots throughout this paper indicate material time derivatives.

3. KINEMATICS

3.1 General Description

The rate-of-deformation (or stretching) tensor in the corotational system is given by:

$$\widehat{d}_{ij} = \frac{1}{2}\left(\frac{\partial \widehat{v}_i}{\partial \widehat{x}_j} + \frac{\partial \widehat{v}_j}{\partial \widehat{x}_i}\right) \tag{13}$$

To evaluate this tensor, we need to obtain the derivatives of the velocity field. From Eqs. 4 and 12 it follows that the velocity field is given by:

$$v = \sum_{I=1}^{4} \left[v_I N_I(\xi,\eta) + \zeta \dot{p}_I N_I(\xi,\eta)\right] \tag{14}$$

Using implicit differentiation, the derivatives of the shape functions are given by:

$$\left\{\begin{array}{c} N_{I,\widehat{x}} \\ N_{I,\widehat{y}} \end{array}\right\} = \frac{1}{J}\left[\begin{array}{cc} \widehat{y}_{,\eta} & -\widehat{y}_{,\xi} \\ -\widehat{x}_{,\eta} & \widehat{x}_{,\xi} \end{array}\right]\left\{\begin{array}{c} N_{I,\xi} \\ N_{I,\eta} \end{array}\right\} \tag{15}$$

where J is the Jacobian. Now using Eq. 4 to express the derivatives of x,y with respect to (x,h), and noting that Eq. 4 holds in any *coordinate* system, we obtain:

$$\left\{\begin{array}{c} N_{I,\widehat{x}} \\ N_{I,\widehat{y}} \end{array}\right\} = \left\{\begin{array}{c} b_{xI} \\ b_{yI} \end{array}\right\} + \overline{\zeta}\left\{\begin{array}{c} b_{xI}^c \\ b_{yI}^c \end{array}\right\} \tag{16}$$

where:

$$\left\{\begin{array}{c} b_{xI} \\ b_{yI} \end{array}\right\} = \frac{1}{J}\left[\begin{array}{cc} \widehat{y}_{,\eta}^m & -\widehat{y}_{,\xi}^p \\ -\widehat{x}_{,\eta}^m & \widehat{x}_{,\xi}^p \end{array}\right]\left\{\begin{array}{c} N_{I,\xi} \\ N_{I,\eta} \end{array}\right\} \tag{17a}$$

$$\left\{\begin{array}{c} b_{xI}^c \\ b_{yI}^c \end{array}\right\} = \frac{1}{J}\left[\begin{array}{cc} p\widehat{y}_{,\eta} & -p\widehat{y}_{,\xi} \\ -p\widehat{x}_{,\eta} & p\widehat{x}_{,\xi} \end{array}\right]\left\{\begin{array}{c} N_{I,\xi} \\ N_{I,\eta} \end{array}\right\} \tag{17b}$$

and

$$J = \det\left[\begin{array}{cc} \widehat{x}_{,\xi}^p + \overline{\zeta}p\widehat{x}_{,\xi} & \widehat{y}_{,\xi}^p + \overline{\zeta}p\widehat{y}_{,\xi} \\ \widehat{x}_{,\eta}^m + \overline{\zeta}p\widehat{x}_{,\eta} & \widehat{y}_{,\eta}^m + \overline{\zeta}p\widehat{y}_{,\eta} \end{array}\right] \tag{17c}$$

As described in Belytschko, Wong and Stolarski (Ref. 6), the terms in J which are linear or higher order in $\overline{\zeta}$ in Eq. 17c have little effect on element performance, so the only term involving $\overline{\zeta}$

which will be retained is the second term in Eq. 16. Thus, using Eqs. 13, 14 and 16 gives the following stretching-velocity relations:

$$\hat{d}_x = \sum_{I=1}^{4} \left[b_{xI}\hat{v}_{xI} + \overline{\zeta}\left(b_{xI}^c\hat{v}_{xI} + b_{xI}\hat{p}_{xI}\right)\right] \tag{18a}$$

$$\hat{d}_y = \sum_{I=1}^{4} \left[b_{yI}\hat{v}_{yI} + \overline{\zeta}\left(b_{yI}^c\hat{v}_{yI} + b_{yI}\hat{p}_{yI}\right)\right] \tag{18b}$$

$$2\hat{d}_{xy} = \sum_{I=1}^{4} \left[b_{xI}\hat{v}_{yI} + b_{yI}\hat{v}_{xI} + \overline{\zeta}\left(b_{xI}^c\hat{v}_{yI} + b_{yI}^c\hat{v}_{xI} + b_{xI}\hat{p}_{yI} + b_{yI}\hat{p}_{xI}\right)\right] \tag{18c}$$

At the quadrature point, $x = h = 0$, the matrix b_{iI} is that given in Belytschko, Lin and Tsay (Ref. 4):

$$\begin{Bmatrix} b_{1I} \\ b_{2I} \end{Bmatrix} = \begin{Bmatrix} b_{xI} \\ b_{yI} \end{Bmatrix} \equiv \begin{Bmatrix} \dfrac{\partial N_I(0,0)}{\partial \hat{x}} \\[2mm] \dfrac{\partial N_I(0,0)}{\partial \hat{y}} \end{Bmatrix} = \frac{1}{2A}\begin{bmatrix} \hat{y}_{24} & \hat{y}_{31} & \hat{y}_{42} & \hat{y}_{13} \\ \hat{x}_{42} & \hat{x}_{13} & \hat{x}_{24} & \hat{x}_{31} \end{bmatrix} \tag{19a}$$

$$A = \frac{1}{2}(x_{31}y_{42} + x_{24}y_{31}) = 4\,J \tag{19b}$$

$$x_{JI} \equiv x_J - x_I \qquad y_{JI} = y_J - y_I \tag{19c}$$

Two methods have been developed to evaluate b_{iI}^c, the terms which couple curvatures to translations. The two methods are distinguished as follows:

1. Method **p** involves the direct evaluation of the second term in Eq. 16; it requires the **p** vectors to be available at all nodes, which is not the case for the Belytschko-Tsay element.
2. Method $\hat{z}$ involves an estimate of these terms based on the assumption of normality of **p** to the surface of the shell; the **p** vectors need not be available.

3.2 Method **p**

In Method **p**, the terms such as $p_{\hat{x},\eta}$ are evaluated directly. The computation is quite simple; from Eq. 4:

$$p_{\hat{x},\eta} = \sum_{J=1}^{4} p_{\hat{x}J}N_{J,\eta} = \frac{1}{4}\sum_{J=1}^{4} p_{\hat{x}J}\eta_J \tag{20}$$

where the last step follows from differentiation of Eq. 11. Hence, using a similar formula for $p_{\hat{x},\xi}$, it follows that:

$$\begin{Bmatrix} b_{xI}^c \\ b_{yI}^c \end{Bmatrix} = \frac{1}{16J} \sum_{K=1}^{4} \begin{Bmatrix} \xi_I p_{\hat{y}K} \eta_K - \eta_I p_{\hat{y}K} \xi_K \\ -\xi_I p_{\hat{x}K} \eta_K + \eta_I p_{\hat{x}K} \xi_K \end{Bmatrix} \tag{21a}$$

$$= \frac{1}{8J} \begin{bmatrix} p_{\hat{y}2} - p_{\hat{y}4} & p_{\hat{y}3} - p_{\hat{y}1} & p_{\hat{y}4} - p_{\hat{y}2} & p_{\hat{y}1} - p_{\hat{y}3} \\ p_{\hat{x}4} - p_{\hat{x}2} & p_{\hat{x}1} - p_{\hat{x}3} & p_{\hat{x}2} - p_{\hat{x}4} & p_{\hat{x}3} - p_{\hat{x}1} \end{bmatrix} \tag{21b}$$

$$I = 1 \qquad I = 2 \qquad I = 3 \qquad I = 4$$

3.3 Method $\hat{z}$

In Method $\hat{z}$, the normal to the mid-surface is first determined. The derivatives of this vector then give b_{iI}^c. To obtain the normal, we start with an expression for the mid-surface based on the bilinear, isoparametric field given by Belytschko and Bachrach (Ref. 2):

$$\hat{z}^m = \sum_{I=1}^{4} (\bar{s}_I + \hat{x} b_{xI} + \hat{y} b_{yI} + \xi \eta \gamma_I) \hat{z}_I \tag{22}$$

$$\bar{s}_I = \frac{1}{4} \left[s_I - b_{xI} \left(\sum_{J=1}^{4} s_J \hat{x}_J \right) - b_{yI} \left(\sum_{J=1}^{4} s_J \hat{y}_J \right) \right] \tag{23a}$$

$$s_J = [1, 1, 1, 1] \tag{23b}$$

$$\gamma_I = \frac{1}{4} \left[h_I - b_{xI} \left(\sum_{J=1}^{4} h_J \hat{x}_J \right) - b_{yI} \left(\sum_{J=1}^{4} h_J \hat{y}_J \right) \right] \tag{23c}$$

$$h_I = [+1, -1, +1, -1] \tag{23d}$$

where b_{iI} are defined in Eq. 19.

The normal to the surface, **p**, is obtained by taking the gradient to the surface described by Eq. 22, which gives:

$$\mathbf{p} = \frac{1}{p^*} \begin{Bmatrix} -\hat{z}_{,\hat{x}} \\ -\hat{z}_{,\hat{y}} \\ 1 \end{Bmatrix} = -\frac{1}{p^*} \sum_{I=1}^{4} \hat{z}_I \begin{Bmatrix} b_{xI} + (\xi \eta)_{,\hat{x}} \gamma_I \\ b_{yI} + (\xi \eta)_{,\hat{y}} \gamma_I \\ -1 \end{Bmatrix} \tag{24a}$$

where:

$$p^* = (1 + \hat{z}_{,\hat{x}}^2 + \hat{z}_{,\hat{y}}^2)^{1/2} \tag{24b}$$

At the origin $(\xi \eta)_{,\hat{x}} = (\xi \eta)_{,\hat{y}} = 0$, because:

$$(\xi \eta)_{,\hat{x}} = \xi \eta_{,\hat{x}} + \xi_{,\hat{x}} \eta = 0 \tag{25}$$

As described earlier, $\mathbf{p}$ by construction is normal to the $\hat{x}$-$\hat{y}$ plane at the origin, so from Eqs. 24a and 25, it follows that:

$$\sum_{I=1}^{4} b_{xI}\hat{z}_I = \sum_{I=1}^{4} b_{yI}\hat{z}_I = 0 \tag{26}$$

Therefore $p^* = 1$ at the origin of the reference plane, i.e. at the quadrature point.

Taking the derivatives of $p_{\hat{x}}$ and $p_{\hat{y}}$ with respect to x and h (and neglecting the terms related to $p_{,\xi}^*$ and $p_{,\eta}^*$, which can be shown to be small) gives:

$$p_{\hat{x},\xi} = -\hat{z}_{,\hat{x}}\hat{x}_{\xi} = -z_\gamma \eta_{,\hat{x}} \tag{27a}$$

$$p_{\hat{x},\eta} = -\hat{z}_{,\hat{x}}\hat{x}_\eta = -z_\gamma \xi_{,\hat{x}} \tag{27b}$$

$$p_{\hat{y},\xi} = -\hat{z}_{,\hat{y}}\hat{y}_\xi = -z_\gamma \eta_{,\hat{y}} \tag{27c}$$

$$p_{\hat{y},\eta} = -\hat{z}_{,\hat{y}}\hat{y}_\eta = -z_\gamma \xi_{,\hat{y}} \tag{27d}$$

where:

$$z_\gamma = \gamma^T \hat{z} = \sum_{I=1}^{4} \gamma_I \hat{z}_I \tag{27e}$$

Since:

$$\begin{bmatrix} \xi_{,x} & \xi_{,y} \\ \eta_{,x} & \eta_{,y} \end{bmatrix} = \frac{1}{J}\begin{bmatrix} y_{,\eta} & -x_{,\eta} \\ -y_{,\xi} & x_{,\xi} \end{bmatrix} = \frac{1}{J}\begin{bmatrix} y_\eta & -x_\eta \\ -y_\xi & x_\xi \end{bmatrix} \tag{28}$$

where:

$$4\hat{y}_\eta = \eta^T \hat{y} = \sum_{I=1}^{4} \eta_I \hat{y}_I \quad \text{etc.} \tag{29}$$

it follows from Eqs. 16, 27 and 28 that:

$$\begin{Bmatrix} b_{xI}^c \\ b_{yI}^c \end{Bmatrix} = \frac{z_\gamma}{16J^2}\begin{Bmatrix} \xi_I \hat{x}_\eta + \eta_I \hat{x}_\xi \\ \xi_I \hat{y}_\eta + \eta_I \hat{y}_\xi \end{Bmatrix} \tag{30a}$$

$$= \frac{2z_\gamma}{A^2}\begin{bmatrix} \hat{x}_{13} & \hat{x}_{42} & \hat{x}_{31} & \hat{x}_{24} \\ \hat{y}_{13} & \hat{y}_{42} & \hat{y}_{31} & \hat{y}_{24} \end{bmatrix} \tag{30b}$$

Thus, this matrix involves the same terms as the $\mathbf{b}$ matrix given in Eq. 19.

Remark. Method $\widehat{z}$ couples curvatures to translations only for warped elements, i.e. when the nodes are not coplanar so that $z_g \neq 0$. Method **p**, on the other hand, also introduces a coupling for surfaces of single curvature. In the latter case, however, the coupling appears to be insignificant.

4. SHEAR PROJECTION

The shear strains are calculated by a nodal projection based on:

$$\overline{\theta}_n^I = \frac{1}{2}\left(\theta_{nI}^I + \theta_{nJ}^I\right) + \frac{1}{L^{IJ}}\left(\widehat{v}_{zJ} - \widehat{v}_{zI}\right) \tag{31}$$

where the superscript I refers to side I and the subscript n refers to a component normal to side I; see Fig. 3.

The transverse shears then are given by:

$$\widehat{\gamma}_{xz} \approx \sum_{I=1}^{4} N_I(\xi, \eta)\overline{\theta}_{\widehat{y}I} \tag{32a}$$

$$\widehat{\gamma}_{yz} \approx -\sum_{I=1}^{4} N_I(\xi, \eta)\overline{\theta}_{\widehat{x}I} \tag{32b}$$

The transverse shears do not depend on w because after the projection, w is considered to have vanished (see Refs. 5 and 15). The terms $\overline{\theta}_{iI}$ are obtained from $\overline{\theta}_n^J$ by the standard transformation:

$$\overline{\theta}_{\widehat{x}I} = \left(e_n^I \cdot e_{\widehat{x}}\right)\overline{\theta}_n^I + \left(e_n^K \cdot e_{\widehat{x}}\right)\overline{\theta}_n^K \tag{33a}$$

$$\overline{\theta}_{\widehat{y}I} = \left(e_n^I \cdot e_{\widehat{y}}\right)\overline{\theta}_n^I + \left(e_n^K \cdot e_{\widehat{y}}\right)\overline{\theta}_n^K \tag{33b}$$

where e_i^* and e_n are unit vectors defined in Fig. 3.

Evaluating the resulting forms for the transverse shear at the quadrature point, $x = h = 0$, gives:

$$\left\{ \begin{array}{c} \widehat{d}_{xz} \\ \widehat{d}_{yz} \end{array} \right\} = \sum_{I=1} \left[\begin{array}{c} b_{xI}^s \\ b_{yI}^s \end{array} \right] \left\{ \begin{array}{c} \widehat{v}_{zI} \\ \widehat{\theta}_{xI} \\ \widehat{\theta}_{yI} \end{array} \right\} \tag{34}$$

$$b_I^s = \frac{1}{4}\left[\begin{array}{ccc} 2(\overline{x}_{JI} - \overline{x}_{IK}) & (\widehat{x}_{JI}\overline{y}_{JI} - \widehat{x}_{IK}\overline{y}_{IK}) & -(\widehat{x}_{JI}\overline{x}_{JI} - \widehat{x}_{IK}\overline{x}_{IK}) \\ 2(\overline{y}_{JI} - \overline{y}_{IK}) & (\widehat{y}_{JI}\overline{y}_{JI} - \widehat{y}_{IK}\overline{y}_{IK}) & -(\widehat{x}_{JI}\overline{y}_{JI} - \widehat{x}_{IK}\overline{y}_{IK}) \end{array} \right] \tag{35}$$

$$\overline{x}_{JI} = \widehat{x}_{JI}/L^{JI} \qquad \overline{y}_{JI} = \widehat{y}_{JI}/L^{JI} \tag{36a}$$

-28-

$$L^{JI} = \hat{x}_{JI}^2 + \hat{y}_{JI}^2 \qquad (36b)$$

5. IMPLEMENTATION

The implementation of this element closely parallels that described in Ref. 4. One-point quadrature is used in conjunction with hourglass control.

The velocity strains for Method $\hat{z}$ in the mid-surface are given by combining Eqs. 18, 19 and 30, which gives:

$$\hat{d}_x^m = (\hat{y}_{24}\hat{v}_{x13} + \hat{y}_{13}\hat{v}_{x42})/(2A) \qquad (37a)$$

$$\hat{d}_y^m = (\hat{x}_{42}\hat{v}_{y13} + \hat{x}_{13}\hat{v}_{y24})/(2A) \qquad (37b)$$

$$2\hat{d}_{xy}^m = (\hat{x}_{42}\hat{v}_{x13} + \hat{x}_{13}\hat{v}_{x24} + \hat{y}_{24}\hat{v}_{y13} + \hat{y}_{31}\hat{v}_{y24})/(2A) \qquad (37c)$$

The curvatures are given by:

$$\kappa_x = (\hat{y}_{24}\hat{\theta}_{y13} + \hat{y}_{13}\hat{\theta}_{y42})/(2A) \qquad (37d)$$

$$+ 2 z_I(\hat{x}_{13}\hat{v}_{x13} + \hat{x}_{42}\hat{v}_{x24})/A^2$$

$$\kappa_y = -(\hat{x}_{42}\hat{\theta}_{x13} + \hat{x}_{13}\hat{\theta}_{x24})/(2A) \qquad (37e)$$

$$+ 2 z_I(\hat{y}_{13}\hat{v}_{y13} + \hat{y}_{42}\hat{v}_{y24})/A^2$$

$$2\kappa_{xy} = (\hat{x}_{42}\hat{\theta}_{y13} + \hat{x}_{13}\hat{\theta}_{y24} - \hat{y}_{24}\hat{\theta}_{x13} - \hat{y}_{31}\hat{\theta}_{x24})/(2A) \qquad (37f)$$

$$+ 2 z_I(\hat{x}_{13}\hat{v}_{y13} + \hat{x}_{42}\hat{v}_{y24} + \hat{y}_{13}\hat{v}_{x13} + \hat{y}_{42}\hat{v}_{x24}$$

The total velocity strains are then computed by:

$$\hat{d}_x = \hat{d}_x^m + \hat{z}\kappa_x \qquad (38)$$

$$\hat{d}_y = \hat{d}_y^m + \hat{z}\kappa_y \qquad (39)$$

$$\hat{d}_{xy} = \hat{d}_{xy}^m + \hat{z}\kappa_{xy} \qquad (40)$$

The hourglass strain rates are computed as in Ref. 4; some modifications are needed to exactly satisfy the patch test. The transverse shear velocity strains are computed as described in the previous section. The stresses s_{ij} and the hourglass stresses Q_1^M, Q_2^M, Q_1^B, Q_2^B and Q_3^B are then computed by the constitutive equation. The nodal force expressions then emanate from the transpose of the kinematic relations.

If the corotational coordinate system $\hat{x}_1, \hat{x}_2$ is updated according to the spin as described in Ref. 4, the rate of the stress corresponds to the Green-Naghdi rate. The formulation thus requires a constitutive law which relates the Green-Naghdi rate to the corotational stretching tensor (Eq. 13). Under these conditions, the formulation is valid for large membrane strains.

6. NUMERICAL STUDIES

6.1 The Patch Test for Explicit Programs

The patch test is of great value in verifying the theoretical validity of elements and their implementation. Unfortunately, it has not been used with explicit programs because the patch test usually is stated as a linear, static problem. This type of problem is not easily treated by nonlinear, explicit transient programs. This section describes a procedure for implementing the patch test in an explicit program which requires no modifications of most programs.

Before describing this procedure, we will describe the standard static patch test, which will clarify our implementation of the dynamic patch test. In the static patch test, an irregular mesh such as shown in Fig. 4 is considered. At the boundary nodes, a displacement field which is consistent with a state of constant strain is prescribed. The displacements of the interior nodes should then be consistent with the linear displacement field associated with this constant strain.

In the plane patch test, the displacements around the periphery of the mesh are prescribed by:

$$u_x = \overline{\alpha}_1 x + \overline{\alpha}_2 y + \overline{\alpha}_3 \qquad (41a)$$

$$u_y = \overline{\alpha}_4 x + \overline{\alpha}_5 y + \overline{\alpha}_6 \qquad (41b)$$

where $\overline{\alpha}_i$ are arbitrary parameters set by the user. Satisfaction of the patch test then requires that in the static solution for this mesh, the displacements of the interior nodes match exactly those given by Eq. 41.

In explicit programs, the implementation of a patch test is hampered by the inability to obtain an exact static solution. Moreover, most explicit programs use rates-of-deformation as a measure of deformation, so prescribing initial displacements will not work. However, these difficulties can be circumvented as follows:

1. Prescribe initial velocities corresponding to Eq. 41 at all nodes of the mesh, i.e.

$$\dot{u}_x = \alpha_1 + \alpha_2 x + \alpha_3 y$$
$$\dot{u}_y = \alpha_4 + \alpha_5 x + \alpha_6 y \qquad (42)$$

2. Integrate one time step with zero body forces.

3. The accelerations should vanish at all interior nodes.

Remark. The constants a_i should be small enough so that any geometric nonlinearities brought into play during the time step are insignificant.

The concept underlying this test is that if Eq. 42 is used as an initial condition on the velocities, then after the first time step, the mesh will displace into the configuration of Eq. 41 with $\overline{\alpha}_i = \alpha_i \Delta t$. The elements should then all have the same constant state of strain and stress, so the accelerations at the interior nodes should vanish. At the boundary nodes, the

accelerations will not vanish because an external force is needed to generate this state of constant stress.

For plate bending, the explicit patch test consists of prescribing $\dot{u}_z$, $\dot{\theta}_x$ and $\dot{\theta}_y$ as follows:

$$\dot{u}_z = \alpha_1 + \alpha_2 x + \alpha_3 y + \alpha_4 x^2 + \alpha_5 xy + \alpha_6 y^2 \qquad (43a)$$

$$\dot{\theta}_x = \frac{\partial \dot{u}_z}{\partial y} = \alpha_3 + \alpha_5 x + 2\alpha_6 y \qquad (43b)$$

$$\dot{\theta}_y = \frac{\partial \dot{u}_z}{\partial x} = \alpha_2 + \alpha_5 y + 2\alpha_4 x \qquad (43c)$$

The system is integrated one time step with zero external loads. The accelerations of interior nodes should then be almost exacly zero, with any deviations ascribable to geometric nonlinearities. If the program is a linear program, they should be exactly zero.

6.2 Twisted Beam

The twisted beam problem is described in Fig. 5. In this problem, we used 5 degrees of freedom per node; 6 degrees of freedom still causes errors. The time history of the displacement at the tip for the in-plane load is given in Fig. 6 and is compared to the Belytschko-Tsay element. As can be seen, the latter diverges immediately; without the additional terms described here, the beam has almost no stiffness. The present element performs very well. Results have been compared to those obtained by the Hughes-Liu element; they differ by less than 1 percent.

6.3 Hemispherical Shell

The mesh for the hemispherical shell is shown in Fig. 7. This mesh differs from the mesh in the MacNeal-Harder test set (Ref. 13) in that there is no hole in the top. Therefore, while in the MacNeal-Harder problem the nodes of each element are coplanar, in this mesh they are not. This has a significant effect on the performance of the element.

As can be seen from Fig. 8, the displacement time history of the Belytschko-Tsay element is quite erratic in this dynamic problem. The improved element, however, behaves perfectly.

6.4 Cylindrical Panel Problem

The last test problem considered here is an impulsively loaded cylindrical panel. The problem description and the mesh are given in Fig. 9. Five integration points were used through the thickness. The number of quadrature points has a sizable effect on the results; marked stiffening is observed when increasing the number of quadrature points from 3 to 5.

A time history of the midpoint deflection is shown in Fig. 10, where it is compared with the experimental results of Balmer and Witmer (Ref. 1) and with results for the Belytschko-Tsay element. The results of the two elements differ little because most of the elements deform into configurations in which the nodes are coplanar. It is only when a significant fraction of the elements is warped that these modifications are important.

7. CONCLUSIONS

Additional terms have been added to the strain-displacement equations of the Belytschko-Tsay element, and the transverse shears have been modified by a projection. These modifications involve hardly any additional computation time; at most, a 10 percent increase in the cost of the element has been observed.

These terms give dramatic improvements in the performance of the element in the twisted beam problem and for a particular meshing of the hemispherical shell problem. In other problems, the differences are insignificant. The terms are important only when the nodes of an element are not coplanar.

An implementation of the patch test for explicit programs has also been described. This element passes the patch test, whereas the Belytschko-Tsay and Hughes-Liu elements do not pass the patch test. Failure to pass the patch test has significant ramifications on the convergence of elements and their performance in distorted meshes.

REFERENCES

1. Balmer, H. A. and Witmer, E. A., "Theoretical - Experimental Correlation of Large Dynamic and Permanent Deformation of Impulsively Loaded Simple Structure," Air Force Flight Dynamics Laboratory, Report FDP-TDR-64-108, 1964.

2. Belytschko, T. and Bachrach, W. E., "Efficient Implementation of Quadrilaterals With High Coarse-Mesh Accuracy," Computer Methods in Applied Mechanics and Engineering, Vol. 54, 1986, pp. 279-301.

3. Belytschko, T. and Tsay, C. S., "Explicit Algorithms for Nonlinear Dynamics of Shells," in Nonlinear Finite Elements Analysis of Plates and Shells, ed. by Hughes, T. J. R., ASME, New York, 1981, pp. 209-231.

4. Belytschko, T., Lin, J. I. and Tsay, C. S., "Explicit Algorithms for the Nonlinear Dynamics of Shells," Computer Methods in Applied Mechanics and Engineering, Vol. 42, 1984, pp. 225-251.

5. Belytschko, T., Stolarski, H. and Carpenter, N., "A C∞ Triangular Plate Element With One-Point Quadrature," International Journal for Numerical Methods in Engineering, Vol. 20(5), 1984, pp. 787-802.

6. Belytschko, T., Wong, B. L. and Stolarski, H., "Assumed Strain Stabilization Procedure for the 9-Node Lagrange Shell Element," International Journal for Numerical Methods in Engineering, Vol. 28(2), 1989, pp. 385-414.

7. Hallquist, J. O., "DYNA3D User's Manual," Report UCID-19592, Rev. 4, Lawrence Livermore National Laboratory, Livermore, Ca., 1988.

8. Hughes, T. J. R. and Liu, W. K., "Nonlinear Finite Element Analysis of Shells: Part I. Three-Dimensional Shells," Computer Methods in Applied Mechanics and Engineering, Vol. 26, 1981, pp. 331-362.

9. Hughes, T. J. R. and Liu, W. K., "Nonlinear Finite Element Analysis of Shells: Part II. Two-Dimensional Shells," Computer Methods in Applied Mechanics and Engineering, Vol. 27, 1981, pp. 167-181.

10. Hughes, T. J. R. and Tezduyar, T. E., "Finite Elements Based Upon Mindlin Plate Theory With Particular Reference to the Four-Node Bilinear Isoparametric Element," Journal of Applied Mechanics, Vol. 48, 1981, pp. 587-596.

11. Liu, W. K., Law, E. S., Lam, D. and Belytschko, T., "Resultant-Stress Degenerated-Shell Element," Computer Methods in Applied Mechanics and Engineering, Vol. 55, 1986, pp. 259-300.

12. MacNeal, R. H., "Derivation of Element Stiffness Matrices By Assumed Strain Distributions," Nuclear Engineering and Design, Vol. 70, 1982, pp. 3-12.

13. MacNeal, R. H. and Harder, R. L., "A Proposed Standard Set of Problems to Test Finite Element Accuracy," Finite Elements in Analysis and Design, Vol. 11, 1985, pp. 3-20.

14. Stanley, G. M., "Continuum-Based Shell Elements," Ph.D. Thesis, Stanford University, Stanford, Ca., 1986.

15. Stolarski, H., Carpenter, N. and Belytschko, T., "A Kirchhoff-Mode Method for C∞ Bilinear and Serendipity Plate Elements," Computer Methods in Applied Mechanics and Engineering, Vol. 50, 1985, pp. 121-145.
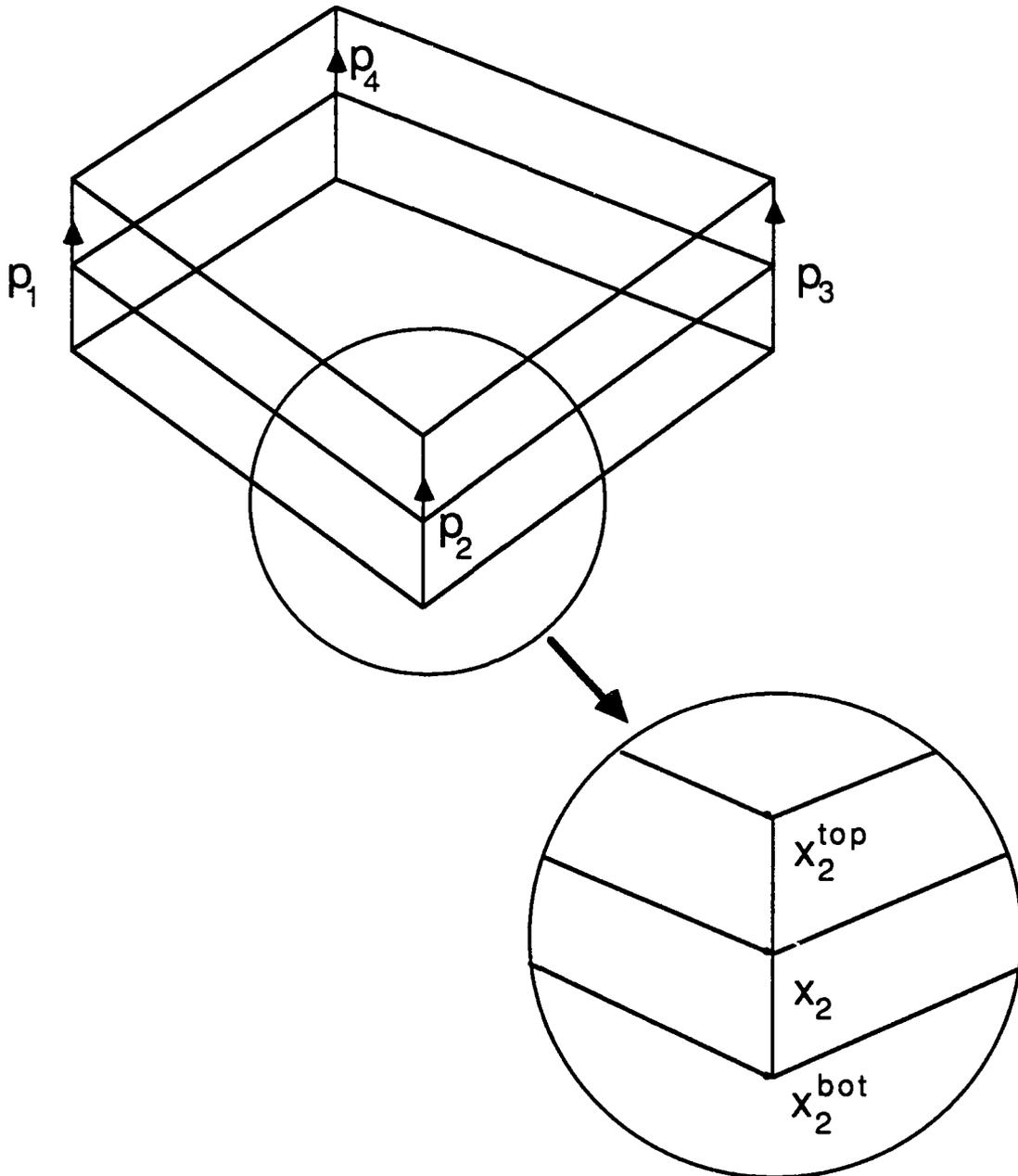
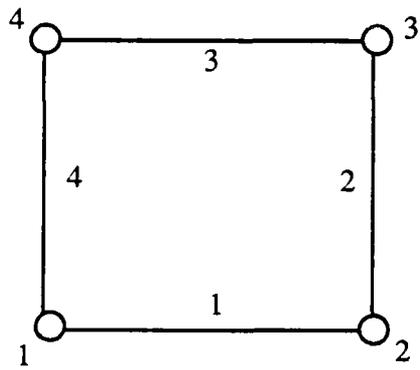Fig. 1 The Geometry of the 4-Node Shell Element and the Degenerated Continum
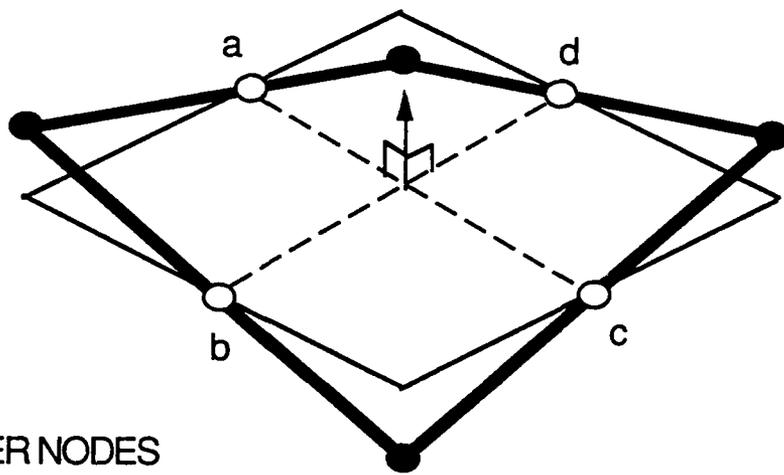
Fig 2 Orientation of Corotational Coordinates.
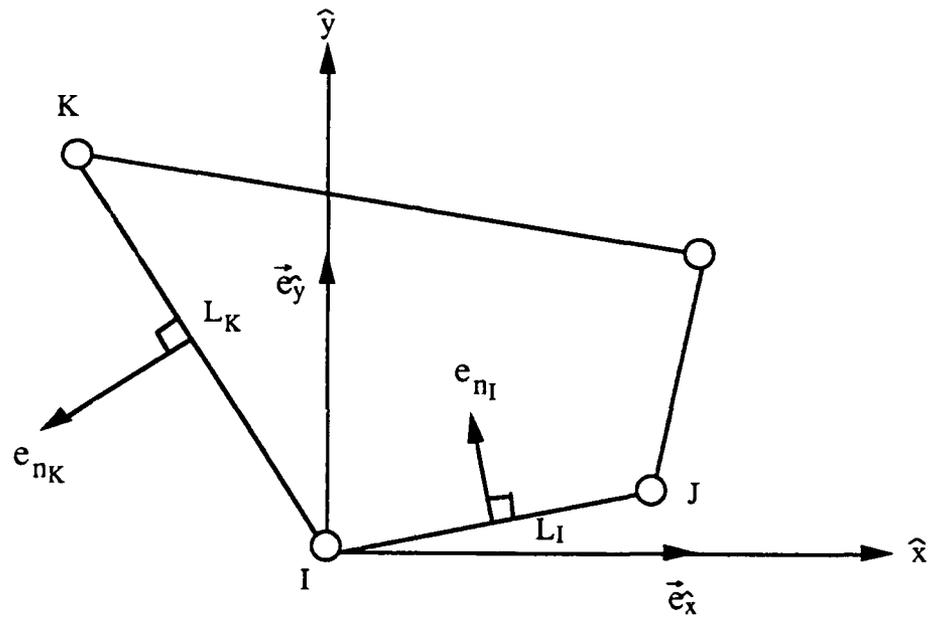
Node and side numbering   Numbering sequence

I	J	K
1	2	4
2	3	1
3	4	2
4	1	3

Fig. 3 Nomenclature for Shear Projection
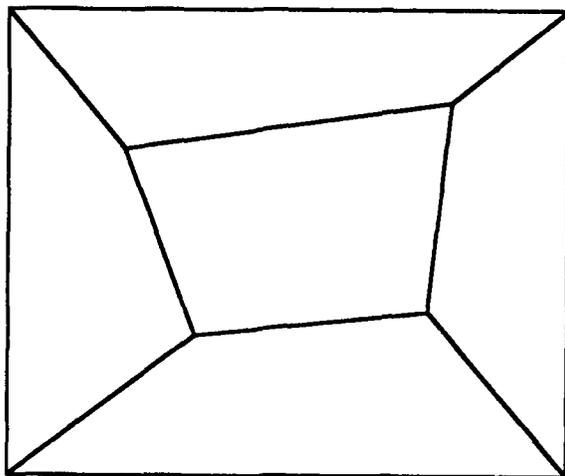
Fig. 4 Mesh for Patch Test.
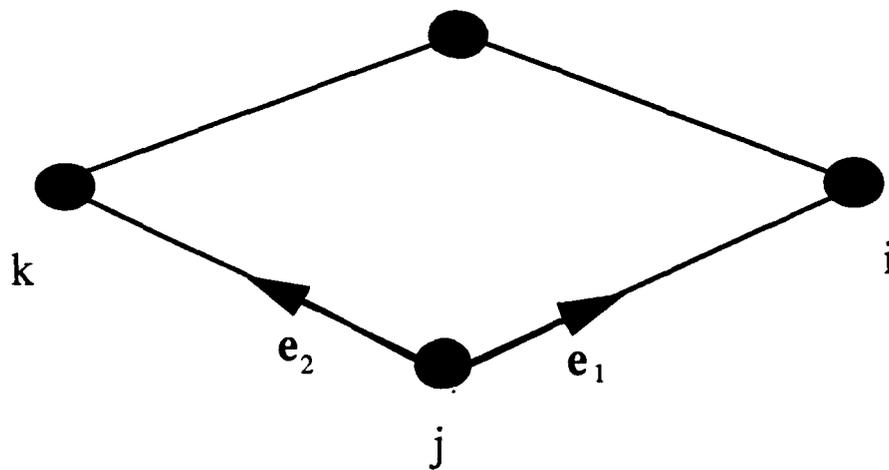
Fig. 5 Local Coordinates for Rotation Projection
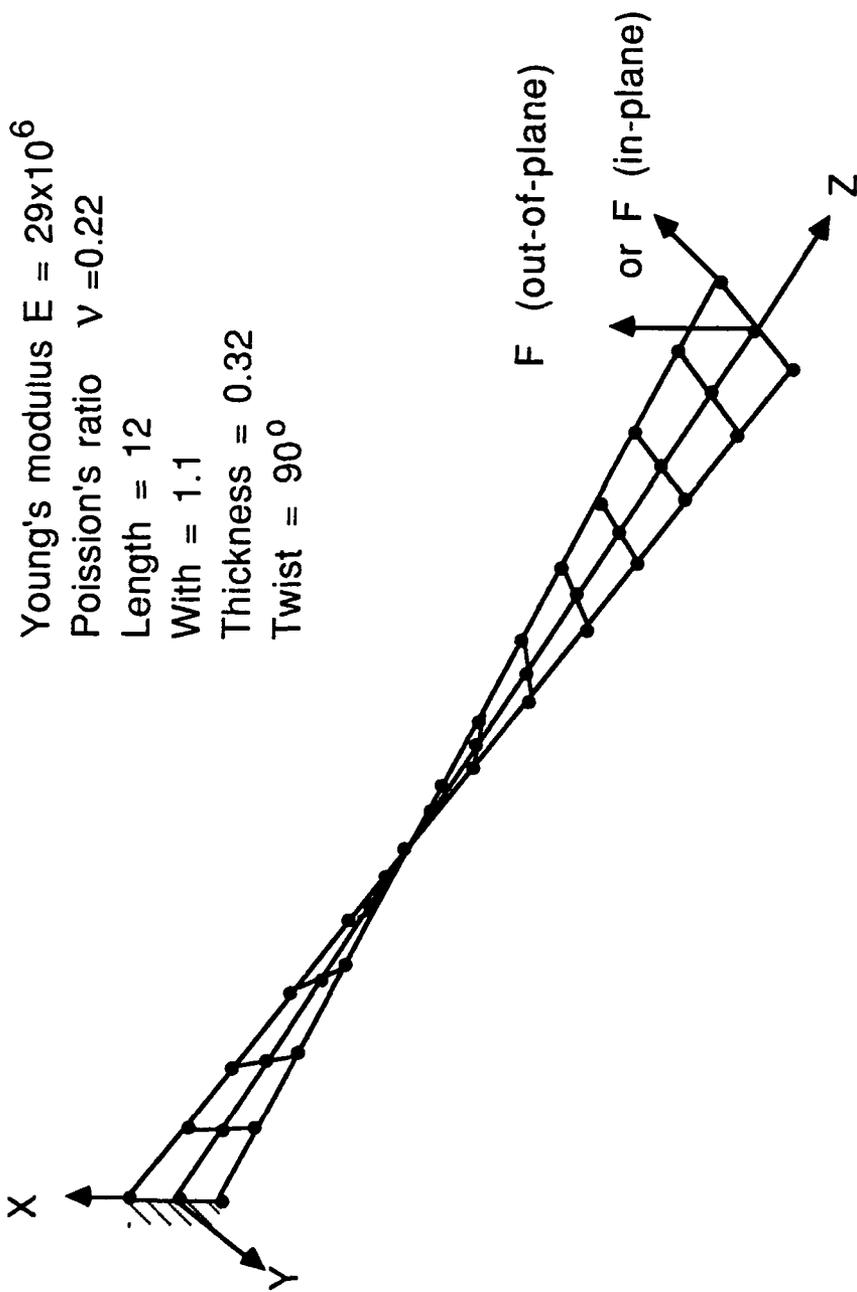
Young's modulus E = 29x10^6
Poission's ratio   V =0.22
Length = 12
With = 1.1
Thickness = 0.32
Twist = 90°

F (out-of-plane)

or F (in-plane)

Z

X

Y

Fig. 6 Mesh and Problem Description for Twisted Beam Problem
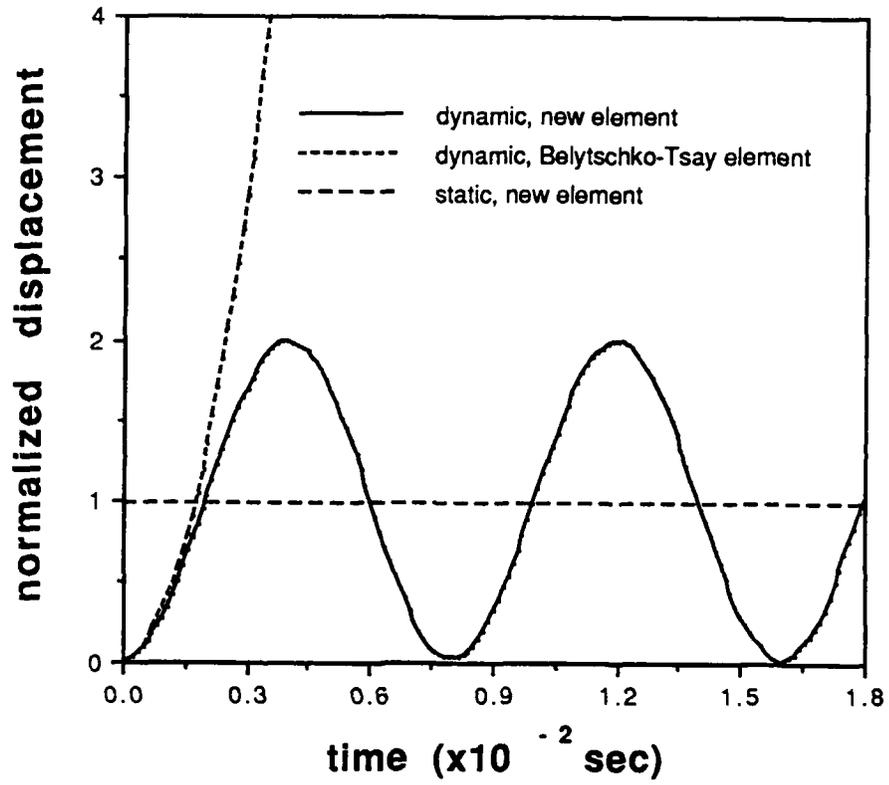
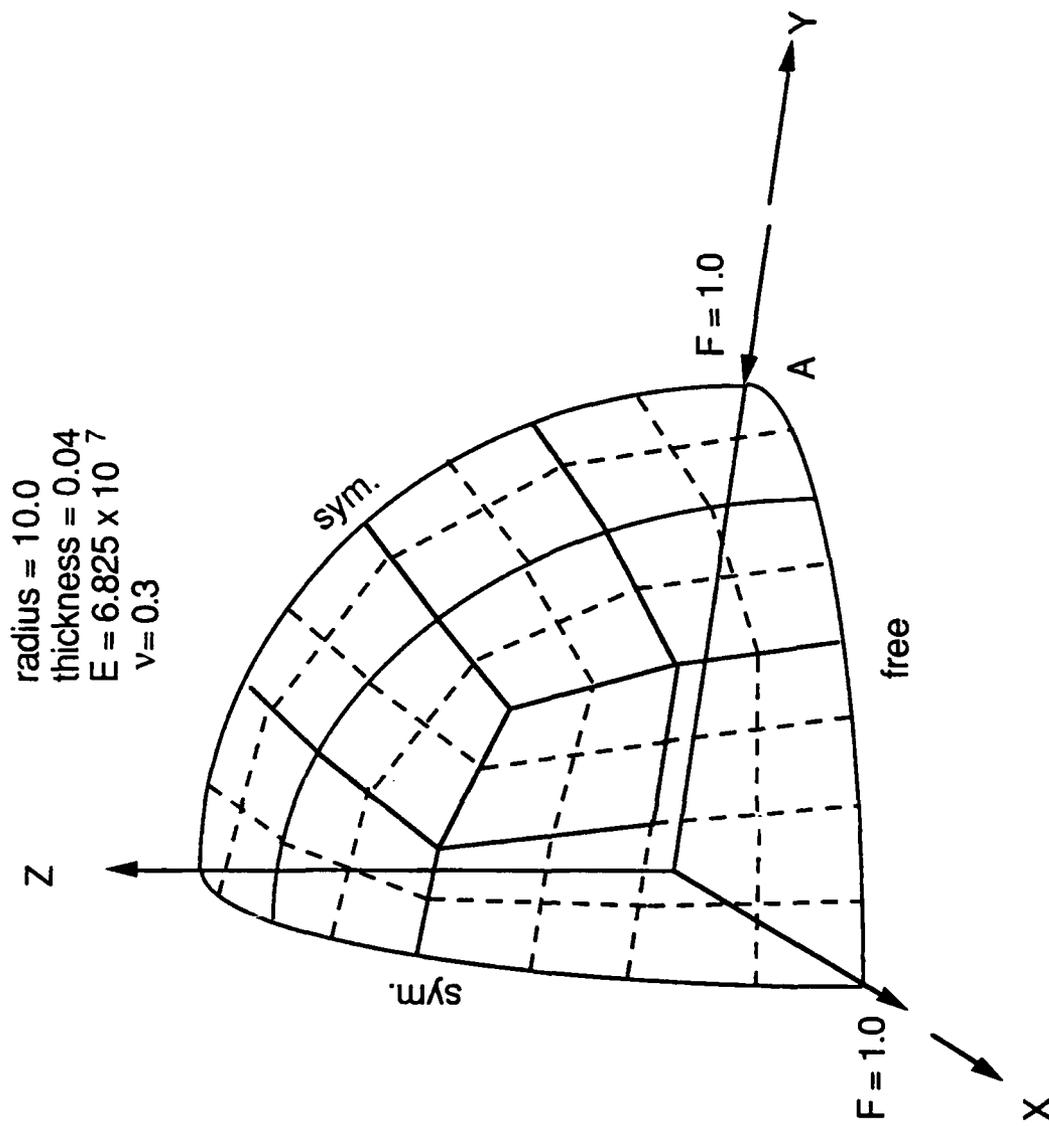Fig 7 Displacement at Tip Normalized to Exact Static Solution

radius = 10.0
thickness = 0.04
$E = 6.825 \times 10^7$
$\nu = 0.3$

sym.

sym.

free

$F = 1.0$

$F = 1.0$

A

X

Y

Z

Fig. 8 Hemispherical Shell Mesh and Problem Description.
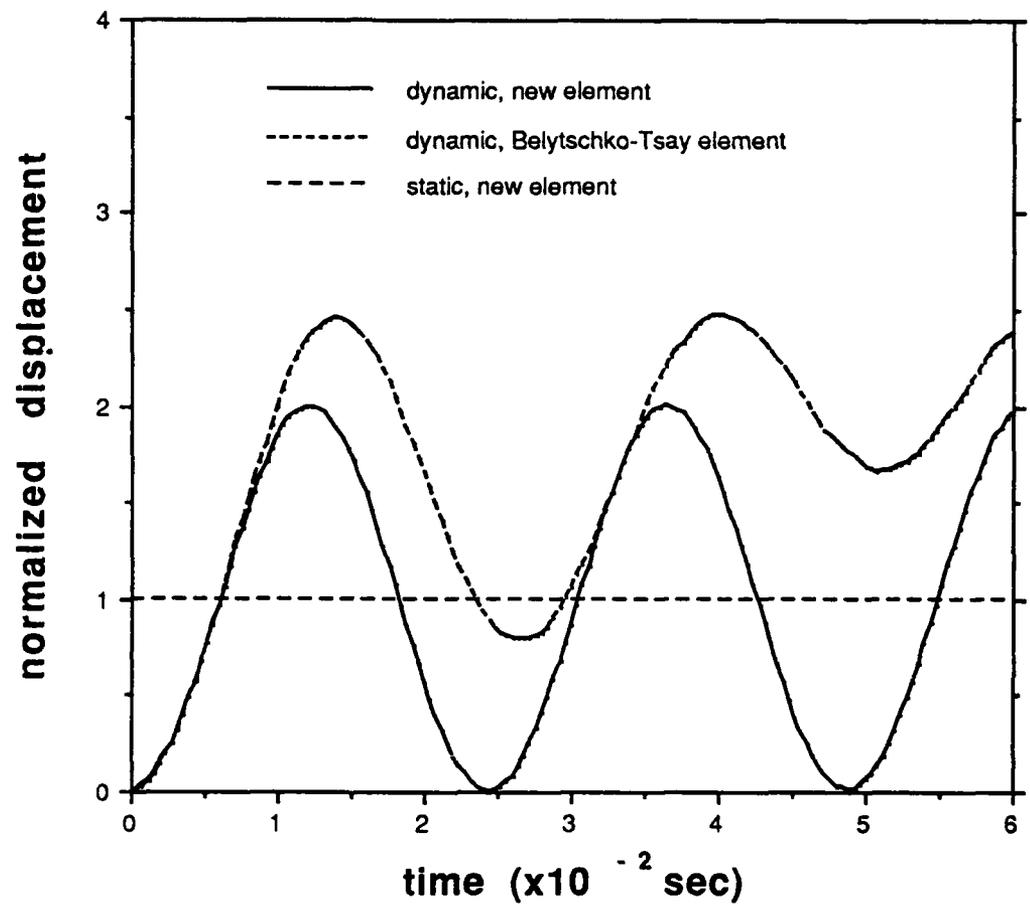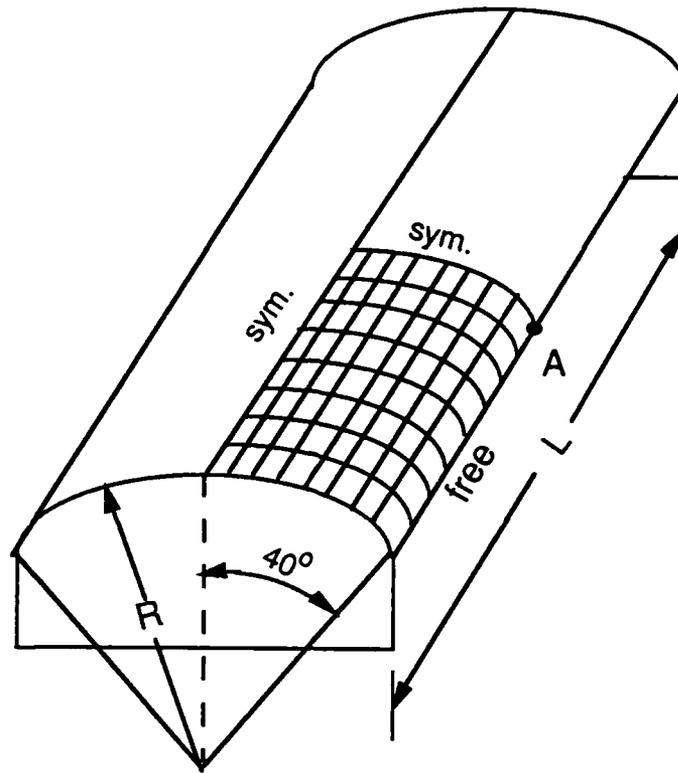
Fig. 9 Displacement Under Load Normalized to Exact Static Solution.

R = 25.0
L = 50.0
thickness = 0.25
E = 4.32 x 10
ν = 0.33
weight = 90.0 per unit area
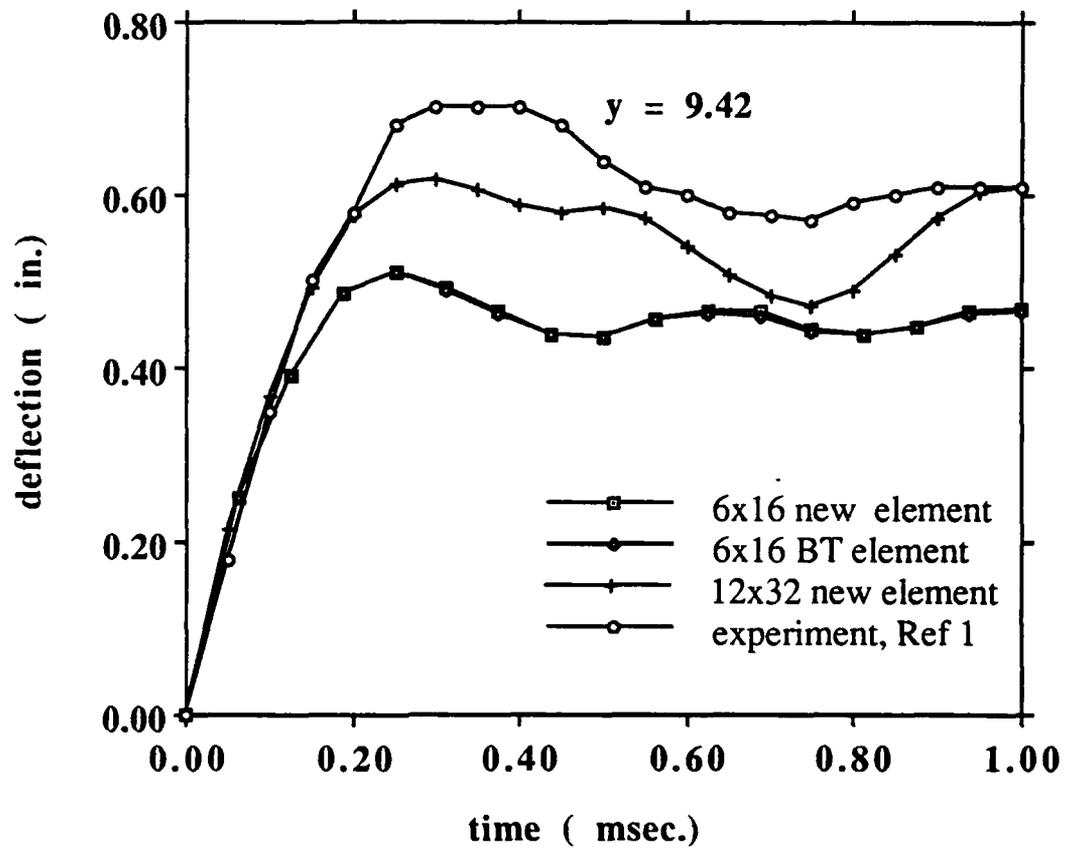
Fig. 10 Impulsively Loaded Cylindrical Panel

Fig. 11 Vertical Displacement of Cylindrical Panel 9.42 in. From Near Support